Terrestrial Planet Formation

John Chambers
Carnegie Institution for Science

The standard planetesimal model of terrestrial-planet formation is based on astronomical and cosmochemical observations, and the results of laboratory experiments and numerical simulations. In this model, planets grow in a series of stages beginning with the μm-sized dust grains observed in protoplanetary disks. Dust grains readily stick together to form mm-to-cm-sized aggregates, some of which are heated to form chondrules. Growth beyond meter size via pairwise sticking is problematic, especially in a turbulent disk. Turbulence also prevents the direct formation of planetesimals in a gravitationally unstable dust layer. Turbulent concentration can lead to the formation of gravitationally bound clumps that become 10–1000 km planetesimals. Dynamical interactions between planetsimals give the largest objects the most favourable orbits for further growth, leading to runaway and oligarchic growth and the formation of Moon-to-Mars-sized planetary embryos. Large embryos acquire substantial atmospheres, speeding up planetesimal capture. Embryos also interact tidally with the gas disk, leading to orbit modification and migration. Oligarchic growth ceases when planetesimals become depleted. Embryos develop crossing orbits, and occasionally collide leaving a handful of terrestrial planets on widely spaced orbits. The Moon probably formed via one such collision. Most stages of planet formation probably took place in the asteroid belt, but dynamical perturbations from the giant planets removed the great majority of embryos and planetesimals from this region.

1. INTRODUCTION

When we think of a planet, our first conception is a body like Earth with an atmosphere, continents, and oceans. However, the Sun's planets are a diverse group of objects that come in several varieties, and extrasolar planets are more diverse still (Figure 1). In this chapter I will focus on terrestrial planets—planets that are mostly composed of refractory materials such as silicates and metal. These objects are large enough to be roughly spherical due to their own gravity. They have a solid surface one could walk around on. They may have an atmosphere, but gases make up a negligible fraction of their total mass.

Terrestrial planets are the only place we know for certain that life can exist. While living organisms might survive on icy satellites like Titan, or in the atmospheres of giant planets, terrestrial planets can provide a number of benefits for life. These include a solid substrate, access to abundant sunlight, and the possibility of liquid water at or near the surface.

Clues to the origin of the Solar System and its planets come from several sources including astronomical observations, data returned from spacecraft, and cosmochemical analysis of samples from planets and asteroids. Numerical simulations are increasingly used to try to make sense of these data and examine different theoretical models for planet formation.

The Sun's planets all orbit in the same direction and have roughly coplanar orbits, suggesting the Solar System formed from a disk-shaped structure. Many young stars are surrounded by Solar-System-sized disks of gas and dust, and these structures are commonly referred to as protoplanetary disks. A typical protoplanetary disk is mostly composed of hydrogen and helium gas. Sub-μm-to-cm-sized dust grains composed of silicates and water ice have been observed in these disks using infrared- and radiotelescopes.

The Sun's protoplanetary disk, also called the solar nebula, must have had a mass of at least 1–2% that of the Sun in order to provide the heavy elements seen in the planets today. However, this "minimum-mass nebula" is only a lower limit—the solar nebula could have been an order of magnitude more massive than this. The solar nebula probably had a composition similar to the Sun itself since most primitive meteorites have fairly similar elemental abundances to the Sun (normalized to silicon) except for highly volatile elements such as hydrogen and the noble gases.

Samples from Earth, the Moon, Mars and most asteroids have roughly uniform isotopic abundances, after physical processes leading to mass-dependent fractionation are taken into account. (Oxygen is a notable exception.) The solar nebula was probably made up of a mixture of material from different stellar sources, which suggests widescale mixing took place, perhaps during an early hot phase. The great depletion of ice-forming elements on the terrestrial planets compared to the outer planets and their satellites suggests the inner nebula was too hot for ices to condense while the inner planets were forming, while the outer nebula must have been cooler.

There are several indications that planets form shortly after stars themselves, and that planet formation is a natural part of star formation. Protoplanetary disks are only seen

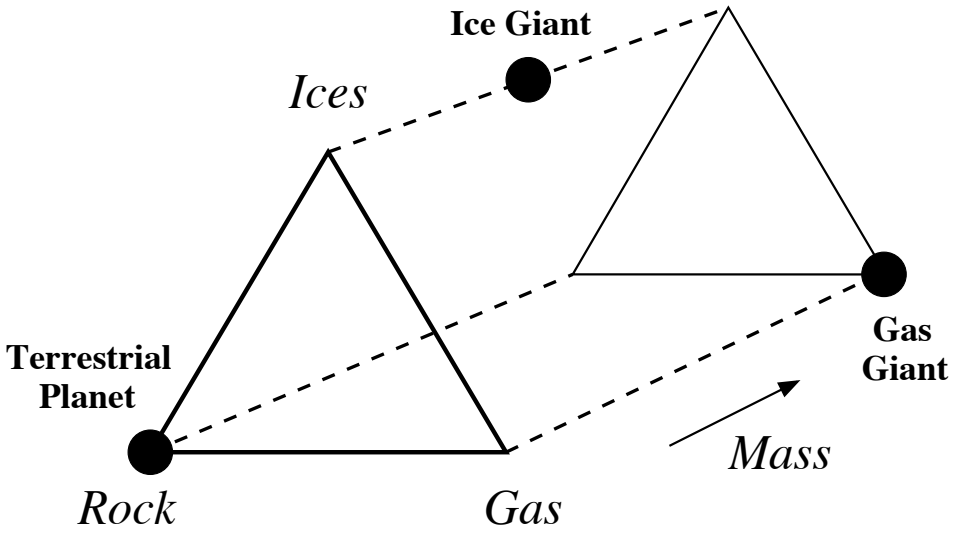

Fig. 1.— Schematic diagram showing different planetary classes seen in the Solar System. Here, 'rock' indicates refractory materials such as silicates, metal, and sulfides; 'ices' refers to ice-forming materials such as water, methane and ammonia, in either solid or fluid form. Other types of planet may exist elsewhere, such as "super Earths"—bodies with masses comparable to Uranus and Neptune but composed almost entirely of rock.

around stars that are thought to be younger than about 10 My. Gas-giant planets like Jupiter, which must acquire most of their mass in gaseous form, have to form while a disk is still present. Disks also provide a way to damp radial and vertical motions that can arise during planet formation, and that would otherwise slow or halt planetary growth. Age measurements using radioactive isotopes suggest the terrestrial planets and asteroids in the Solar System took less than 200 My to form, and are roughly 4.5 Gy old, which matches estimates for the age of the Sun based on stellar evolution models.

The ancient surfaces of the Moon, Mercury, Mars, and some of the satellites of the giant planets are covered in impact craters, which suggests collisions played a much more important role in the early Solar System than they do today. This observation and the abundance of dust grains seen in protoplanetary disks has given rise to the planetesimal model for planet formation, which infers that planets formed as a result of numerous collisions between small objects to form larger ones. The asteroid belts between Mars and Jupiter, and beyond the orbit of Neptune, can be thought of as leftover material from this collisional epoch that was prevented from growing into additional planets.

The planetesimal hypothesis is widely accepted today as the basis of terrestrial planet formation. It remains unclear whether gas-giant planets also form this way. The standard version of this model may require some modification in light of the growing variety of extrasolar planetary systems that are being discovered. In particular, the fact that many extrasolar planets lie close to their parent star or have highly eccentric orbits argues that a planet's orbit can change substantially during or after its formation. It is plausible that extrasolar systems will contain new types of planet that do not exist in the Solar System, and these objects may have rather different formation histories than Earth.

2. FOUNDATIONAL CONCEPTS AND EQUATIONS

2.1 Dust Dynamics

In a protoplanetary disk with a composition similar to the Sun, roughly 99% of the initial mass is gas, primarily hydrogen and helium. The remaining 1% of the mass exists in solid grains that are $\sim 1\,\mu$m in size. These dust grains provide the starting point for the formation of terrestrial planets.

As dust grains orbit the star, they interact with the gas in the disk, experiencing aerodynamic drag forces. The strength of this interaction can be characterized by the stopping time:

$$t_{\rm stop} \equiv \frac{M|v - v_{\rm gas}|}{F_{\rm drag}} \qquad (1)$$

where M is the mass of a dust grain, and v and $v_{\rm gas}$ are the velocity of the grain and the gas respectively.

The drag force $F_{\rm drag}$ varies depending on the size and shape of a particle. For a spherical particle with radius $R < 9\lambda/4$, where λ is the mean free path of the gas molecules, the particle undergoes Epstein drag:

$$F_{\rm drag} = -\left(\frac{\rho_{\rm gas} c_s}{\rho R}\right) M(v - v_{\rm gas}) \quad (2)$$

where $\rho_{\rm gas}$ and c_s are the density and sound speed of the gas, and ρ is the density of the particle. For larger spherical objects, the drag force is

$$F_{\rm drag} = -\frac{3 C_D \rho_{\rm gas}}{8 \rho R} M(v - v_{\rm gas})|v - v_{\rm gas}| \quad (3)$$

The drag coefficient C_D depends on the Reynolds number Re, and is approximately given by:

$$\begin{aligned} C_D &\simeq 24{\rm Re}^{-1} && {\rm Re} < 1 \\ &\simeq 24{\rm Re}^{-0.6} && 1 < {\rm Re} < 800 \\ &\simeq 0.44 && {\rm Re} > 800 \end{aligned} \quad (4)$$

where

$${\rm Re} \equiv \frac{2R|v - v_{\rm gas}|}{\nu_m} \quad (5)$$

and $\nu_m \simeq \lambda c_s/2$ is the molecular viscosity (Weidenschilling 1977, Cuzzi et al 1993). Note that the last of Eqns. 4 corresponds to Stokes drag. The stopping time increases with particle size, so small particles are more tightly coupled to the motion of the gas than large ones.

Very small dust grains undergo Brownian motion due to collisions with individual gas molecules. The typical relative velocity for grains of mass M can be determined from approximate equipartition of kinetic energy:

$$v_{\rm rel} \simeq \left(\frac{M_m}{M}\right)^{1/2} c_s \quad (6)$$

where M_m is the mass of a gas molecule.

Grains also sediment towards the midplane of the disk due to the vertical component of the star's gravity, moving at terminal vertical velocity $v_{\rm settle}$ determined by a balance between gravity and gas drag:

$$v_{\rm settle} = -\Omega^2 z t_{\rm stop} \quad (7)$$

where z is the distance from the midplane and Ω is the orbital angular frequency. Large particles settle faster than small ones, allowing them to sweep up material as they fall.

Gas density, pressure, and temperature in a disk all tend to decrease radially with distance from the star. The outward pressure gradient means that gas orbits the star at slightly less than the Keplerian orbital velocity of a solid body:

$$v_{\rm gas} = \Omega r(1 - \eta) \quad (8)$$

where r is the distance from the star. The factor η can be calculated by balancing the gravitational, centrifugal and pressure forces on a parcel of gas, giving:

$$\eta = -\frac{1}{2\rho_{\rm gas}\Omega^2 r}\frac{dP}{dr} \quad (9)$$

The reduced orbital velocity of the gas means that dust particles experience a headwind and lose angular momentum. As a result, particles drift radially through the disk towards the star or the nearest pressure maximum. Particles drift inwards at a velocity determined by a balance between stellar gravity, gas pressure, and centrifugal and Coriollis forces, where:

$$\frac{dr}{dt} \simeq -\frac{2\eta r}{t_{\rm stop}}\left[\frac{(\Omega t_{\rm stop})^2}{1 + (\Omega t_{\rm stop})^2}\right] \quad (10)$$

(Weidenschilling 1977). Drift rates are highest when $\Omega t_{\rm stop} = 1$, which corresponds to roughly m-sized particles. In this case, particles move inwards by 1 AU every 10^2–10^3 years, and this rapid drift poses a challenge for models of planet formation. Particles continue drifting until they collide with another object or reach a region that is hot enough for them to evaporate.

Protoplanetary disks are likely to be turbulent, at least in some locations. Turbulence provides a way to drive the viscous evolution of disks and the observed accretion of material onto the central star. However, the mechanism that sustains turbulence is unclear. The turbulent viscosity ν is often assumed to have the form

$$\nu = \alpha c_s H_{\rm gas} \quad (11)$$

where $H_{\rm gas} \simeq c_s/\Omega$ is the vertical scale height of the gas disk, and $\alpha \leq 1$ is a parameter that depends on the mechanism driving the turbulence (Shakura and Sunyaev 1973). This is equivalent to saying that the horizontal shear stress on a parcel of gas in the disk is approximately α times the gas pressure. The form of Eqn. 11 was originally justified on the assumption that turbulence in disks has a hydrodynamic origin such as thermal convection. It is less clear whether the same form will apply for other sources of turbulence. As a result, α probably varies in time and space in real disks. Observed accretion rates in protoplanetary disks suggest $\alpha \sim 10^{-2}$–10^{-3} on average (Hartmann et al. 1998, Hueso and Guillot 2005).

The largest turbulent eddies in a disk probably rotate at an angular frequency Ω_L that is no slower than Ω, due to the Coriolis force. The size L and rotational velocity V_L of the largest eddies are related via the viscosity, such that $\nu \simeq L V_L$. This implies that $V_L \sim c_s\sqrt{\alpha}$ and $L \sim H_{\rm gas}\sqrt{\alpha}$ (Cuzzi et al. 2001). Turbulence typically follows a Kolmogorov energy spectrum, which can be derived from dimensional analysis, such that an eddy with radius l has a rotational velocity

$$v_l = l\Omega_l \sim V_L\left(\frac{l}{L}\right)^{1/3} \quad (12)$$

where Ω_l is the angular frequency of the eddy (Cuzzi and Weidenschilling 2006). As a result, gas moves more slowly in small eddies than in large ones. The size of the smallest eddy is set by the point at which collisions between gas molecules smooth out turbulent motions.

Particles couple strongly to large eddies with $\Omega_l \ll 1/t_{\rm stop}$. Neighboring particles moving in the same eddy have similar velocities. Particles couple poorly to small eddies with $\Omega_l \gtrsim 1/t_{\rm stop}$, and undergo a randomly fluctuating acceleration instead. In this case, neighboring particles will have different velocities even if the particles are the same size. Since v_l increases with l, the relative velocities between equally sized particles will be greatest when $\Omega_L t_{\rm stop} = 1$. These objects will have $R \sim 1$ m if $\Omega_L \sim \Omega$.

Larger objects will also be affected by turbulent fluctuations, but the accelerations will be smaller due to their greater inertia. For all sizes, the velocity of a particle due to turbulence, relative to a body moving on a circular Keplerian orbit, is roughly

$$v_{\rm turb} \sim \frac{V_L}{(1 + t_{\rm stop}/t_L)^{1/2}} \tag{13}$$

where $t_L = 2\pi/\Omega_L$ (Cuzzi et al. 1993).

2.2 Dust Grain Collisions

Most of what we know about collisions between dust grains comes from laboratory experiments. Poppe et al. (2000) have found that individual, uncharged, spherical silica grains, stick together due to electrostatic forces when they collide at low speeds. At high speeds, grains collide and rebound. There is a fairly sharp transition between these two regimes. The dividing line depends on particle radius, and lies at ~ 1 m/s for μm-sized grains. Irregularly shaped grains behave differently: the probability of sticking versus rebound declines with increasing collision speed, but there is no sharp transition. Some collisions can lead to sticking at speeds of up to 50 m/s (Poppe et al. 2000).

Dust collision experiments in microgravity show that low-velocity collisions ($\ll 1$ m/s) lead to the formation of loose fractal aggregates with fractal dimension ~ 2 (Blum and Wurm 2000). At larger impact speeds, sticking still occurs but growth is accompanied by compaction as grain-grain bonds break and grains start to roll over one another. At collision speeds $\gtrsim 1$ m/s, individual grains are ejected from loose aggregates. Still more energetic collisions catastrophically disrupt an existing aggregate (Blum and Wurm 2000).

Collisions involving compacted aggregates of dust grains are somewhat different. When mm-to-cm-sized aggregates of μm-sized grains collide at speeds of a few m/s, they rebound with the loss of some individual grains. However above ~ 10 m/s, small aggregates embed themselves in larger ones. Some fragments escape from the larger aggregate but it gains mass overall (Wurm et al. 2005).

Many meteorites are primarily composed of rounded mm-sized particles called chondrules. These appear to be dust aggregates that were heated in the solar nebula and partially or completely melted. Experiments designed to reproduce chondrule textures suggest that they cooled slowly over a period of hours (Connelly and Jones 2005). These slow cooling rates suggest chondrules formed in dense regions of the nebula, with high solid-to-gas ratios, possibly in shocks.

Collisions between monolithic objects like chondrules differ from those between loosely bound dust aggregates. Typically, low-speed collisions lead to rebound, while collisions above ~ 20 m/s lead to some fragmentation (Ueda et al. 2001). The presence of fine dust grains in chondrule-forming regions allowed chondrules to accrete thick dust rims in 10^2–10^3 years (Cuzzi 2004). These porous dust rims help chondrules stick together during collisions, as compaction of the rims absorbs impact energy (Ormel et al. 2008). This process ceases once all the dust is accreted and the rims become compacted, at which point the largest compounds are likely to be < 1 m in radius.

Numerical simulations show that in the absence of turbulence μm-sized dust grains aggregate into m-sized bodies in $\sim 10^4$ orbital periods for plausible sticking probabilities (Weidenschilling 1997). Growth mainly occurs when large aggregates sweep up small ones. Without turbulence, similarly-sized objects have low relative velocities, so mutual collisions are not disruptive, even though they may not lead to growth.

In a turbulent nebula, meter-sized objects collide with one another at substantial speeds, probably leading to fragmentation rather than growth. Meter-sized particles also have short drift lifetimes, severely limiting the amount of time available to grow into larger objects. These difficulties suggest that growth may stall when objects reach ~ 1 m in diameter, a problem referred to as the "meter-size barrier". This issue is discussed further in Section 3.1

2.3 Gravitational Instability

In the absence of turbulence, dust grains will gradually sediment towards a thin layer at the disk midplane. Perturbations in this layer can potentially grow in size leading to gravitational instability. This has long been considered as a possible mechanism for the formation of planetesimals (Goldreich and Ward 1973) although this issue remains controversial.

A perturbation in the density of the particle layer with frequency ω satisfies a dispersion relation given by

$$\omega^2 = k^2 v_{\rm rel}^2 + \Omega^2 - 2\pi G \Sigma_{\rm solid} k \tag{14}$$

where $\Sigma_{\rm solid}$ is the surface density of particles, $v_{\rm rel}$ is their velocity dispersion, and $k = 2\pi/\lambda$ where λ is the wavelength of the perturbation (Goldreich and Ward 1973). The dust layer becomes unstable when $\omega^2 \leq 0$, which occurs for some values of λ when

$$v_{\rm rel} \leq \frac{\pi G \Sigma_{\rm solid}}{\Omega} \tag{15}$$

The largest region that can become unstable (the case where $v_{\rm rel} \simeq 0$) is

$$\lambda_{\rm max} \simeq \frac{4\pi^2 G \Sigma_{\rm solid}}{\Omega^2} \tag{16}$$

If the particles in this clump collapse to form a solid body, this object will have a mass given by

$$M_{\rm max} \sim \Sigma_{\rm solid} \lambda_{\rm max}^2 \tag{17}$$

However this is only a very rough guide to the size of object that may form by gravitational instability. Complete collapse may be prevented by random motions or rotation, so that only part of a gravitationally unstable clump collapses. For particles with $\Omega t_{\rm stop} \ll 1$, it may take many orbital periods for the particles to sediment to the centre of a clump (Cuzzi and Weidenschilling 2006), and neighboring clumps may merge during this time.

Settling of dust grains to the midplane is opposed by intrinsic turbulence in the disk. As a vertical concentration gradient develops, turbulent diffusion tends to move particles away from the midplane again. A rough estimate for the scale height $H_{\rm solid}$ of the particle layer comes from assuming settling and turbulence are in equilibrium:

$$\left(\frac{H_{\rm solid}}{H_{\rm gas}} \right)^2 \simeq \frac{\alpha}{\Omega t_{\rm stop}(1 + \Omega t_{\rm stop})} \tag{18}$$

(Cuzzi and Weidenschilling 2006). Intrinsic turbulence generally prevents gravitational instability unless the particles are large or α is very small.

Dust settling can generate turbulence in an otherwise laminar disk. When the mass of solid particles near the midplane exceeds that of the gas, the particles begin to drag the gas along at the Keplerian velocity $v_{\rm kep} = \Omega r$. Gas above and below the midplane orbits at sub-Keplerian speeds $v_{\rm kep}(1-\eta)$ due to the radial pressure gradient in the disk. This vertical velocity shear generates turbulence that opposes further dust settling (Weidenschilling 1980). Gravitational instability is probably prevented by shear induced turbulence except in regions where $\Sigma_{\rm solid} \sim \Sigma_{\rm gas}$ (Garaud and Lin 2004) or in parts of the disk where there is no radial pressure gradient.

2.4 Runaway and Oligarchic growth

Although it is currently unclear how planetesimals formed, it is assumed they did so in large numbers at an early stage in the solar nebula. Two new mechanisms that may generate planeteimals in a turbulent disk are described in Section 3.1.

Once planetesimals are present, mutual collisions can lead to growth or fragmentation depending on the strength of the objects and the impact velocity. Collisions can take place in one of two size regimes depending on whether gravity is an important factor.

Monolithic bodies with radius $R \lesssim 100$ m have negligible gravitational fields. These objects tend to grow weaker with increasing size since big bodies typically contain larger flaws than small bodies. The tensile stress required to activate a flaw decreases with the length of the flaw, so large bodies break apart at lower impact speeds than smaller bodies. Collisions involving large bodies also last longer, so there is more time for flaws to grow and coalesce (Housen and Holsapple 1999).

Impact strength is often characterized using $Q_S^\star$, which is the kinetic energy per unit target mass required to break up a body such that the largest fragment contains half the original mass of the target. Experiments and numerical simulations find that

$$Q_S^\star \propto R^{-b_s} \tag{19}$$

where $b_s \simeq 0.4$—0.6 for rock and water ice, while the constant of proportionality depends on the material (Housen and Holsapple 1999, Benz and Asphaug 1999). The outcome of a collision also depends on the mass ratio of the projectile and target. For a given projectile kinetic energy, low velocity collisions involving large projectiles are more disruptive than high velocity impacts by small projectiles (Benz 2000).

Bodies with $R \gtrsim 100$ m become harder to disrupt with increasing size because fragments need to be ejected rapidly enough to escape from the object's gravitational field. The impact strength in this regime is characterized using $Q_D^\star$, which is the energy per unit target mass required to break up and disperse the body so that the largest reaccumulated object contains half the mass of the target. Numerical simulations suggest that

$$Q_D^\star \propto \rho R^{b_g} v^c \tag{20}$$

where $b_g \simeq 1.2$–1.5 for rock and water ice, and $c \sim 0.5$ (Melosh and Ryan 1997, Benz and Asphaug 1999, Benz 2000). Again there is a dependence on the impact velocity v, and hence on the projectile to target mass ratio. Objects are most easily disrupted when they are hit by large, slow moving projectiles.

Initially, planetesimals were probably loosely compacted aggregates rather than monolithic bodies. In the strength regime ($\lesssim 100$ m in size), aggregates are weaker than monolithic bodies since energy that would go into breaking the object instead goes into dispersing the pre-existing pieces (Benz 2000). Aggregates can actually be stronger than monoliths in the gravity regime, in some cases, since shockwaves propagate less effectively through aggregates (Asphaug et al. 1998). Planetesimals that formed within the first 2 My in the solar nebula, and grew larger than a few tens of km, probably melted and differentiated due to heat released by short-lived radioactive isotopes such as ^{26}Al (Woolum and Cassen 1999). These objects would have behaved as monoliths rather than aggregates, although energetic impacts may subsequently have converted them into gravitationally bound "rubble piles". The values of $Q_S^\star$ and $Q_D^\star$ for real planetesimals are poorly constrained at present.

In both the strength and gravity regimes, the mass of the largest surviving body (which may consist of gravitationally

reaccumulated fragments) is

$$\frac{M_{\rm largest}}{(M_{\rm target}+M_{\rm projectile})} \simeq 0.5 + s(1-\frac{Q}{Q_D^\star}) \qquad (21)$$

where Q is the kinetic energy of the projectile per unit target mass and $s \sim 0.5$ (Benz and Asphaug 1999). Thus, low energy collisions lead to net growth while high energy collisions lead to erosion. In a size distribution of planetesimals, large objects are more likely to grow via collisions while small planetesimals may be disrupted.

When planetesimals are large enough to have appreciable gravitational fields, they focus the trajectories of other passing objects towards them, increasing the chance of a collision. From conservation of energy and angular momentum, the collision probability is increased by a gravitational focussing factor:

$$F_{\rm grav} = 1 + \left(\frac{v_{\rm esc}}{v_{\rm rel}}\right)^2 \qquad (22)$$

where $v_{\rm esc}$ is the escape velocity and $v_{\rm rel}$ is the relative velocity of the objects when they are far apart.

The growth rate of a planetesimal of mass M and radius R, moving through a population of smaller bodies of radius $R_{\rm small}$ can be calculated by determining the volume of space that the planetesimal moves through, modifying for gravitational focussing:

$$\frac{dM}{dt} = \frac{\pi(R+R_{\rm small})^2 \Sigma_{\rm solid} v_{\rm rel}}{2H_{\rm solid}} F_{\rm grav} F_{\rm 3B} \qquad (23)$$

where we have assumed that the mass of escaping fragments is negligible. Here $\Sigma_{\rm solid}$ and $H_{\rm solid}$ are the surface density and vertical scale height of the planetesimal disk. In deriving this equation, we have neglected the fact that planetesimals actually travel on curved orbits about the central star. For an ensemble of planetesimals with a range of eccentricities e and inclinations i, the presence of the star increases the collision probability for those objects with small e and i. This can be accounted for with a correction factor $F_{\rm 3B} \sim 3$ for the mean growth rate (Greenzweig and Lissauer 1992).

When e and i are very small, the gravitational reach of a planetesimal can become larger than the scale height of the particle disk. In this case, the problem is essentially two dimensional, and the growth rate becomes:

$$\frac{dM}{dt} = 2(R+R_{\rm small})\Sigma_{\rm solid} v_{\rm rel}\left(1+\frac{v_{\rm esc}^2}{v_{\rm rel}^2}\right)^{1/2} \qquad (24)$$

Gravitational interactions between planetesimals with different masses causes dynamical friction, which tends to equipartition the kinetic energy associated with radial and vertical motions. If equipartition of energy goes to completion

$$\begin{aligned} Me^2 &\simeq \text{constant} \\ Mi^2 &\simeq \text{constant} \end{aligned} \qquad (25)$$

so large bodies have small e and i, and vice versa. In practice, equipartition is not reached, partly because close encounters tend to increase e and i for all bodies (referred to as viscous stirring), and also because gas drag continually damps e and i at rates that depend on an an object's size.

Gas drag damping rates are roughly

$$\begin{aligned} \frac{de}{dt} &\simeq -\frac{e}{t_{\rm stop}}\left(\eta^2+\frac{5}{8}e^2+\frac{1}{2}i^2\right)^{1/2} \\ \frac{di}{dt} &\simeq -\frac{i}{2t_{\rm stop}}\left(\eta^2+\frac{5}{8}e^2+\frac{1}{2}i^2\right)^{1/2} \end{aligned} \qquad (26)$$

where the gas drag time is

$$t_{\rm stop} = \frac{8\rho R}{3C_D\rho_{\rm gas} v_{\rm rel}} \qquad (27)$$

where $v_{\rm rel}$ is the velocity of the object with respect to the gas, and $C_D \sim 1$ for planetesimal-sized bodies (Adachi et al. 1976).

During the early stages of growth, viscous stirring rates are determined by the mean planetesimal mass, which changes slowly over time. As a result, $v_{\rm rel}$ also changes slowly. Eventually $F_{\rm grav}$ becomes large for some objects since $v_{\rm esc} \propto M^{1/3}$. Neglecting the first term on the right-hand side of Eqn. 22, the growth rate for the largest planetesimals becomes

$$\frac{dM}{dt} \propto \Sigma_{\rm solid} M^{4/3} \qquad (28)$$

from Eqn. 23, where we have assumed that $H_{\rm solid} \propto v_{\rm rel}$. The corresponding growth timescale is

$$t_{\rm grow} \sim M/\frac{dM}{dt} \propto \frac{1}{M^{1/3}} \qquad (29)$$

Under these circumstances, large planetesimals grow faster than small ones, a situation called runaway growth. Dynamical friction gives large bodies nearly circular, coplanar orbits, so these bodies have large gravitational focussing factors. Conversely, $F_{\rm grav}$ is smaller for low-mass bodies and these grow more slowly.

Runaway growth ceases when the largest bodies become massive enough to control the velocity distribution of the smaller planetesimals. This happens when the mass of the largest objects $M_{\rm large}$ satisfies

$$2M_{\rm large}\Sigma_{\rm Large} \gtrsim \bar{M}\Sigma_{\rm solid} \qquad (30)$$

where $\bar{M}$ is the mean planetesimal mass (Ida and Makino 1993).

At this point, an approximate balance between viscous stirring and gas drag means that $v_{\rm rel}$ for the small planetesimals depends on the mass of the largest body in their vicinity, such that $v_{\rm rel} \propto M_{\rm large}^{1/3}$ (Thommes et al. 2003). The growth rate of the largest planetesimals now becomes

$$\frac{dM}{dt} \propto \Sigma_{\rm solid} M^{2/3} \qquad (31)$$

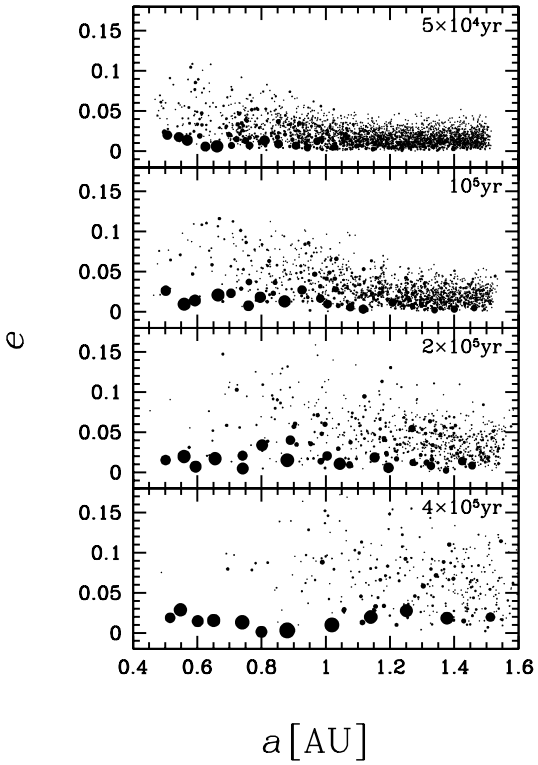

Fig. 2.— A numerical simulation of oligarchic growth beginning with 10,000 equal-mass planetesimals with a total mass 2.5 times that of Earth. The panels show 4 snapshots in time. Each circular symbol shows the orbital semi-major axis a and eccentricity e of a planetesimal, with symbol radius proportional to the planetesimal's radius. Figure kindly supplied by Eiichiro Kokubo.

from Eqn. 23, and the corresponding growth timescale is

$$t_{\rm grow} \sim M/\frac{dM}{dt} \propto M^{1/3} \tag{32}$$

A new regime called oligarchic growth is established, in which each region of the disk tends to be dominated by a single large body called a planetary embryo (Figure 2). Equation 32 shows that the masses of neighboring embryos tend to converge over time. All embryos grow faster than a typical planetesimal because they have larger gravitational focussing factors. Embryos typically maintain non-overlapping orbits with a separation bR_H, where the Hill radius R_H is a measure of the gravitational reach of the embryo, given by

$$R_H = a\left(\frac{M}{3M_\star}\right)^{1/3} \tag{33}$$

where a is the semi-major axis of the orbit, and $b \sim 10$ (Kokubo and Ida 1998). Embryos typically collide with one another when $b \ll 10$ so that their wide spacing is maintained.

Embryos primarily accrete planetesimals from an annulus a few Hill radii wide centred on their orbit, called a feeding zone. The width of a feeding zone is proportional to $M^{1/3}$, while the surface density of planetesimals in the feeding zone declines with M. As a result, the maximum mass of an embryo is finite, even if no other embryos are present. An embryo that accretes all the mass in its feeding zone reaches its isolation mass, given by

$$M_{\rm iso} = \left(\frac{8\pi^3\Sigma_{\rm solid}^3 a^6 b^3}{3M_\star}\right)^{1/2} \tag{34}$$

The isolation mass will be modified if solid material moves radially through the disk, for example via gas drag for planetesimals, or planetary migration for embryos. Oligarchic growth usually ceases before the embryos reach $M_{\rm iso}$ since dynamical friction weakens as planetesimals are consumed, and embryos no longer have nearly circular, non-overlapping orbits (Kenyon and Bromley 2006). In the Solar System, the runaway and oligarchic growth stages probably lasted 10^5–10^6 years after planetesimals formed (Wetherill and Stewart 1993, Kokubo and Ida 2000). At the end of the oligarchic growth stage, embryos at 1 AU from the Sun would have had masses of 0.01–0.1$M_\oplus$ for plausible values of $\Sigma_{\rm solid}$.

2.5 Late-Stage Growth

When planetary embryos reach roughly the mass of Mars, they acquire thick atmospheres of gas captured from the surrounding disk. Planetesimals passing through an atmosphere are slowed, increasing the probability of capture. Using a rough estimate for the energy lost due to gas drag, the atmospheric density needed to capture a planetesimal of

radius R and density ρ is

$$\rho_{\rm gas}(r) \simeq \frac{2R\rho}{3r_H}\left(\frac{24+5e^2/h^2}{24}\right) \quad (35)$$

where r_H is the Hill radius of the embryo, $h = r_H/a$, and e is the orbital eccentricity of the planetesimal (Inaba and Ikoma 2003, Chambers 2006).

An accurate determination of the enhanced collision cross section of an embryo requires a detailed atmospheric model. However, in the inner regions of a purely radiative atmosphere, with a mass that is negligible compared to the embryo, the density at a distance r from the centre of the embryo is roughly:

$$\rho_{\rm gas} \sim \frac{\rho_0}{W_0}\left(\frac{V_0}{4}\right)^3\left(\frac{R_0}{r}\right)^3 \quad (36)$$

where

$$\begin{aligned} V_0 &= \frac{RM\rho_0}{R_0P_0} \\ W_0 &= \frac{3\kappa LP_0}{4\pi a_r cGMT_0^4} \end{aligned} \quad (37)$$

where R_0 is the outer radius of the atmosphere where it meets the surrounding nebula, T_0, P_0 and ρ_0 are the temperature, pressure and density at this outer radius, a_r is the radiation density constant, κ is the atmospheric opacity due mainly to dust grains, and L is the luminosity due mainly to energy released from impacting planetesimals (Inaba and Ikoma 2003).

Above a critical mass, an embryo's gravity is too strong to maintain a static atmosphere. This mass is approximately

$$M_{\rm crit} \sim 7\left(\frac{\dot{M}}{1\times10^{-7}M_\oplus/{\rm y}}\right)^{s_1}\left(\frac{\kappa}{1\ {\rm cm}^2/{\rm g}}\right)^{s_2} M_\oplus \quad (38)$$

where κ is the opacity of the atmosphere, $\dot{M}$ is the rate at which the embryo is accreting mass in the form of planetesimals, and $s_1 \simeq 1/4$ and $s_2 \simeq 1/4$ (Ikoma et al. 2000). Gas from the disk flows onto objects with $M > M_{\rm crit}$, providing one pathway to giant-planet formation. For small values of $\dot{M}$ and κ, Earth-mass bodies can exceed the critical mass, however gas accretion rates are extremely low for such bodies (Ikoma et al. 2000).

A planet interacts tidally with gas in the disk, generating torques that can alter the planet's orbit. Interactions are particular important at Lindblad resonances, where the orbital frequency of the gas $\Omega_{\rm gas}$ is related to that of the planet by

$$m(\Omega_{\rm gas} - \Omega_{\rm planet}) = \pm\kappa_e \quad (39)$$

where $\kappa_e \simeq \Omega_{\rm gas}$ is the epicyclic frequency, and m is an integer. At a Lindblad resonance, gas moving on an eccentric orbit always has conjunctions with the planet at the same phase in its orbit, enhancing the planetary perturbation. Interactions can also be important at the corotation resonance, where $\Omega_{\rm gas} = \Omega_{\rm planet}$, although this tends to be less important than the Lindblad resonances for terrestrial-mass planets.

Tidal interactions with the gas disk have two effects: they damp a planet's orbital eccentricity and inclination, and they alter the semi-major axis of the orbit. The latter effect is commonly referred to as "type-I" planetary migration (another kind of migration, "type-II", affects giant planets). In a non-magnetic, vertically isothermal disk, these changes are

$$\begin{aligned} \frac{da}{dt} &= -(2.7-1.1x)\left(\frac{c_s}{v_{\rm kep}}\right)^2\frac{a}{t_{\rm tidal}} \\ \frac{de}{dt} &= -0.780\frac{e}{t_{\rm tidal}} \\ \frac{di}{dt} &= -0.544\frac{i}{t_{\rm tidal}} \end{aligned} \quad (40)$$

where

$$t_{\rm tidal} = \left(\frac{M_\star}{M}\right)\left(\frac{M_\star}{\Sigma_{\rm gas}a^2}\right)\left(\frac{c_s}{v_{\rm kep}}\right)^4 \quad (41)$$

and $\Sigma_{\rm gas} \propto a^x$ (Tanaka et al. 2002, Tanaka and Ward 2004).

Damping of e and i happens on a timescale that is 2–3 orders of magnitude shorter than that for changes in a. Even so, inward migration can be rapid: an Earth-mass planet at 1 AU has an inward migration timescale of $\sim 10^5$ years in a minimum-mass nebula.

Equations 40 were derived for an idealized case. The magnitude and direction of migration in real disks are highly uncertain at present. Migration rates may be reduced or reversed in non-isothermal disks where the planetary perturbation on the gas is taken into account (Paardekooper and Mellema 2006). Inward migration is also slowed in regions where the disk opacity changes rapidly (Menou and Goodman 2004), or in the presence of a toroidal magnetic field (Fromang et al. 2005). Migration is likely to be outward rather than inward in regions containing steep, positive surface density gradients, such as those at the edge of an inner cavity in the disk (Masset et al. 2006).

In a turbulent disk, turbulent density fluctuations in the gas can generate torques on a planet's orbit that change a, e and i. These fluctuations typically change on timescales comparable to the orbital period, so the long-term effect is that the orbit undergoes a random walk, sometimes referred to as stochastic migration (Nelson 2005). Unlike smooth tidal torques, stochastic migration is potentially important for low-mass objects like planetesimals. In particular, it is likely to raise the relative velocities of planetesimals, potentially reducing growth rates and increasing collisional fragmentation.

Protoplanetary disks typically disperse after a few My, probably due to a combination of viscous accretion onto the star and photoevaporation (Haish et al. 2001, Alexander et al. 2006). At this point, tidal damping of e and i ceases. Dynamical friction with planetesimals also becomes much

TABLE 1
MAXIMUM ECCENTRICITIES OF THE INNER PLANETS FROM CONSERVATION OF ANGULAR MOMENTUM DEFICIT

Planet	$e_{\max}$	$q_{\min}$ (AU)	$Q_{\max}$ (AU)
Mercury	0.409	0.229	0.545
Venus	0.093	0.656	0.790
Earth	0.077	0.923	1.077
Mars	0.212	1.201	1.847

less effective as planetesimals are removed and oligarchic growth ends. At this point, the terrestrial-planet region of the solar nebula probably still contained 10–100 embryos. Perturbations between neighboring embryos increase e and i causing their orbits to cross. The number of embryos is gradually reduced due to mutual collisions, while residual planetesimals are swept up. This process continues until the remaining objects have non-crossing orbits that are stable for the age of the star.

The time required to form Earth can be estimated from Eqn. 23 noting that $H \simeq v_{\rm rel}/\Omega$ and $F_{\rm grav} \simeq F_{\rm 3B} \simeq 1$ after oligarchic growth ceases, so that:

$$t_{\rm late} = M/\left(\frac{dM}{dt}\right) \sim \frac{4R\rho}{3\Sigma_{\rm solid}\Omega} \qquad (42)$$

At 1 AU from the Sun, assuming that $\Sigma_{\rm solid} \sim 4$ g/cm^2 when oligarchic growth ceased, gives $t_{\rm late} \sim 2 \times 10^8$ years. This is roughly consistent with estimates based on radioactive dating (see Section 3.2).

A system of 2 planets of mass M_1 and M_2 orbiting a star of mass $M_\star$ is stable against collisions if the energy and angular momentum satisfy

$$-\frac{2M_{\rm tot}EJ^2}{G^2M_{\rm prod}^3} > 1 + 3^{4/3}\frac{M_1M_2}{M_\star^{2/3}(M_1+M_2)^{4/3}} + \cdots \qquad (43)$$

where $M_{\rm tot}$ is the total mass of the system, E is the total energy, J is the total angular momentum, and $M_{\rm prod} = M_\star(M_1+M_2) + M_1M_2$ (Gladman 1993).

For three or more planets, there is no known analytic stability criterion. However, numerical simulations have provided an approximate empirical way to gauge instability. Planets with mass M, on initially circular orbits, develop crossing orbits on a timescale $t_{\rm cross}$ given by

$$\log t_{\rm cross} \sim Bb + C \qquad (44)$$

where b is the mean orbital separation in Hill radii, and $B \propto M^{1/12}$ and C are constants that depend on the number of planets N and planetary mass, although B is roughly independent of N for $N \geq 5$ (Chambers et al. 1996). Extrapolating this relation would suggest that a system of four terrestrial-mass planets would be stable for the age of the Solar System if their mean orbital separation was $b \sim 12$. The inner planets are actually spaced further apart than this by factors of 3–5. This may reflect evolutionary processes during their formation, but it must also partly be due to the fact that the orbits of the planets are not circular.

An approximate way to gauge the stability of eccentric orbits is by considering their angular momentum deficit (AMD), which is the difference between the angular momentum and that of a circular orbit with the same semi-major axis:

$$\mathrm{AMD} = M(GM_\star a)^{1/2}(1 - \sqrt{1-e^2}\cos i) \qquad (45)$$

For a system of planets on widely spaced orbits, AMD is approximately constant since the total angular momentum is conserved and the semi-major axes change only slightly. In the Solar System, angular momentum transfer between the inner and outer planets is relatively inefficient, so to a first approximation, the AMD of the inner planets is roughly constant over Gy timescales (Laskar 1997). However, AMD is readily exchanged between the inner planets, resulting in changes in e and i. The maximum value of e for each planet occurs when it absorbs the entire AMD for the system. These values of e are shown in Table 1, together with the resulting perihelion and aphelion distances q and Q respectively. It appears that the inner planets will probably avoid a collision over the age of the Solar System. However, that this is not a rigorous constraint since some AMD exchange with the outer planets does take place.

Collisions between embryos do not always result in a merger. Oblique impacts between similarly sized embryos can have a high specific angular momentum. If the embryos merged to form a single body the rotation frequency may exceed the critical value at which rotational break up occurs:

$$\omega_{\rm crit} \simeq \left(\frac{4\pi G\rho}{3}\right)^{1/2} \qquad (46)$$

Numerical simulations show that pairs of embryos involved in oblique collisions often separate again at greater than their mutual escape velocity, exchanging some material during the collision (Agnor and Asphaug 2004). Head-on collisions do not suffer from this problem, but at high impact speeds, embryo-embryo collisions can lead to net erosion rather than growth. Mercury may have experienced such a collision that stripped away much of its rocky mantle leaving a high-density planet with a relatively large iron-rich core (Benz et al. 1988).

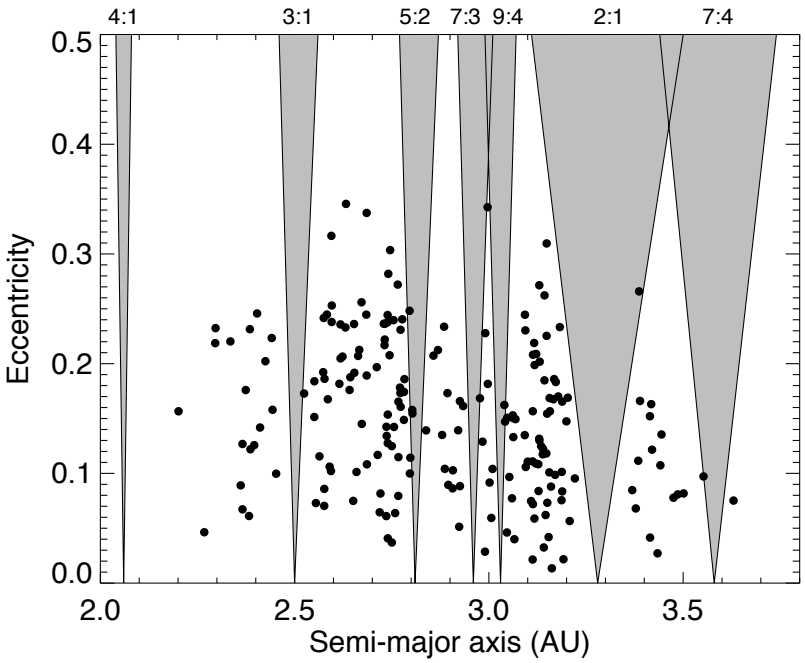

Fig. 3.— Orbits of main-belt asteroids larger than 100 km in diameter, and approximate locations of the major mean-motion resonances with Jupiter. The resonance regions are typically empty. The ν_6 secular resonance removes asteroids with semi-major axes $2.0 \lesssim a \lesssim 2.2$ AU. Adapted from Nesvorný et al. (2002).

The Moon probably formed as a result of an oblique impact between a Mars-mass embryo and Earth towards the end of its accretion. Numerical simulations show that if the two bodies were already differentiated, their iron cores would coalesce. However, tidal torques from the non-spherical distribution of mass would have ejected a substantial amount of rocky material, mostly from the impactor, into orbit around Earth forming a disk (Canup and Asphaug 1999, Canup 2004). Unlike many bodies in the Solar System, Earth and the Moon have identical oxygen isotope ratios (Wiechert et al. 2001), which suggests there was substantial exchange of material between Earth and the protolunar disk (Pahlevan and Stevenson 2007). Mass in the disk would have quickly coalesced into the Moon provided it was beyond the Roche radius, given by

$$R_{\rm Roche} \simeq 2.44 \left(\frac{\rho_\oplus}{\rho_{\rm disk}} \right)^{1/3} \tag{47}$$

where $\rho_{\rm disk}$ is the mean density of material in the disk. Subsequent tidal evolution rapidly expanded the Moon's orbit and slowed Earth's rotation.

Runaway and oligarchic growth probably took place in the asteroid belt but no planet exists there today. Compositional differences between meteorites show they come from at least several dozen different parent asteroids (Meibom and Clark 1999), so the asteroids do not represent the remains of a single planet. The asteroid belt is highly depleted in mass compared to other regions of the Solar System with a total mass of $\sim 1/2000 M_\oplus$. This suggests most of the primordial mass in this region was removed either before or after it formed into planets. Collisional fragmentation probably played only a minor role in removing this mass for several reasons. These include the preservation of an almost intact basaltic crust on asteroid 4 Vesta, the small number of impact-generated satellites around large asteroids (Durda et al. 2004), and the paucity of impact events between the formation of the asteroid belt and the onset of the late heavy bombardment ~ 4 Gy ago as recorded in meteorites (Bogard 1995).

The asteroid belt probably lost most of its mass dynamically due to gravitational perturbations from the giant planets. Perturbations are especially effective at resonances. A mean-motion resonance (MMR) between 2 objects occurs when

$$p_1 n_1 + p_2 n_2 + p_3 \dot{\varpi}_1 + p_4 \dot{\varpi}_2 = 0 \tag{48}$$

where $n_i = 2\pi/P_i$, where P is the orbital period, ϖ_i is the longitude of periapse of planet i, and the p_j are integers such that $\sum p_j = 0$. Since the orbital precession period is usually much longer than the orbital period, an approximate condition for a MMR is that the two periods are related by

$$\frac{P_1}{P_2} \simeq -\frac{p_1}{p_2} \tag{49}$$

A secular resonance occurs when the periapse or nodal

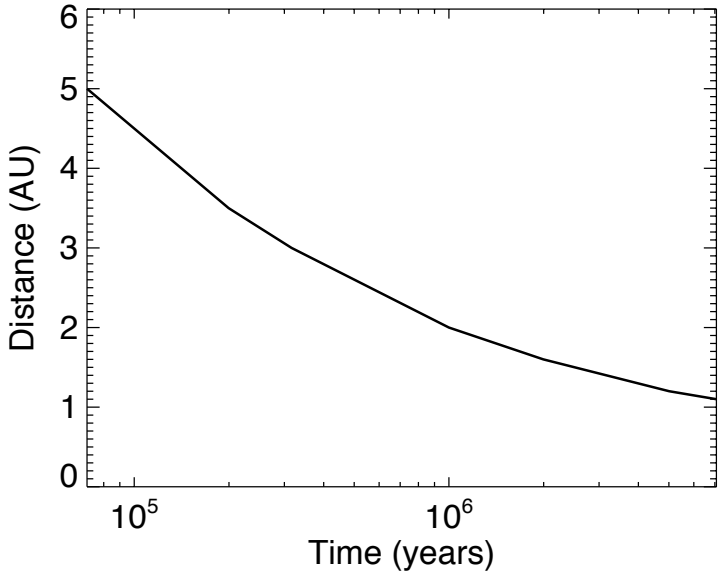

Fig. 4.— Approximate location of the ice line in the solar nebula over time. Adapted from Kennedy and Kenyon (2008).

precession frequency of an object matches one of the eigenfrequencies ν of the linearized secular equations for the planetary system. In the asteroid belt, the most important secular resonances are

$$\begin{aligned} \dot{\varpi} &= \nu_5 \simeq \dot{\varpi}_J \\ \dot{\varpi} &= \nu_6 \simeq \dot{\varpi}_S \\ \dot{\Omega} &= \nu_{16} \simeq \dot{\Omega}_S \end{aligned} \quad (50)$$

where in this instance Ω refers to the longitude of the ascending node of an orbit, and ϖ_J, ϖ_S and Ω_S are the longitudes of perihelion of Jupiter and Saturn and the longitude of the ascending node of Saturn, respectively (Murray and Dermott 2000).

An asteroid located in a MMR typically has a highly chaotic orbit because multiple sub-resonances (different values of p_3 and p_4) are located close to one another and these resonances overlap. For these orbits, e increases stochastically on a timescale of ~ 1 My, until the object collides with the Sun or a planet, or has a close encounter with Jupiter, leading to hyperbolic ejection (Gladman et al. 1997). Secular resonances cause a monotonic increase in e and lead to the same outcome.

Resonances currently occupy a small fraction of the asteroid belt (Figure 3), but their importance in the early Solar System was increased by two factors. While the nebula was still present, its gravity modified the resonance locations. As the nebula dispersed, the resonances moved radially, sweeping across the asteroid belt, and potentially removing a large fraction of the planetesimals and planetary embryos that were present (Lecar and Franklin 1997, Nagasawa et al. 2000). Secondly, if planetary embryos were present in the asteroid belt, their mutual perturbations would have occasionally nudged one of them into a resonance, increasing the fraction of objects removed (Chambers and Wetherill 2001).

2.6 Chemical Evolution

Models for the solar nebula suggest the inner few AU may initially have been hot enough to vaporise most minerals (Boss 1996). However, protoplanetary disks cool over time as energy released by viscous accretion and the luminosity of the central star both decline. Table 2 shows some of the materials that would condense as the temperature decreased in the solar nebula. This condensation sequence assumes a C/O number density ratio $\simeq 0.5$ equivalent to that in the Sun. In a disk with C/O > 1, oxides and silicates would be replaced by carbides and nitrides. At low temperatures, chemical reactions may be kinetically inhibited so the mixture of solids will not necessarily reach an equilibrium (Lewis and Prinn 1980). As a result, it is unclear what the dominant C and N bearing species will be in cool regions of a disk. In the inner solar nebula, these elements mainly existed as gases.

The inner planets and all meteorites, except CI chondrites, are depleted in moderately volatile elements such as sodium and sulphur, relative to silicon, compared to the Sun. In chondritic meteorites, the degree of depletion is roughly correlated with an element's volatility, but the pattern differs from one group of meteorites to another. These depletion patterns may be a signature of incomplete condensation of these elements from a gradually cooling nebula (Cassen 1996). As the nebula cooled, it continued to lose

gas, so the more volatile elements were under represented when planetesimals formed. Alternatively, the depletions may be a signature of thermal processing of solids in the nebula, perhaps associated with chondrule formation. The lack of isotopic fractionation in elements such as potassium (Humayun and Clayton 1995), and the partial retention of elements such as sodium argues that chondrule formation must have occurred in regions with high dust/gas densities in this case (Alexander et al. 2008).

Beyond a certain distance from the star, temperatures in a protoplanetary disk are cold enough for water ice to condense. This location is called the ice line. Over time, the ice line and other condensation fronts move closer to the star as the disk cools, so the composition of solid material at a given location changes (see Figure 4). Chondrule ages measured using radioactive isotope systems show that chondrule formation spanned several My in the solar nebula, which suggests that planetesimals also formed over a range of times. Planetesimals that formed in the same location at different times would have had different compositions because local nebula conditions would have changed. Similarly, planetesimals forming concurrently at different distances from the star would have different compositions.

Main-belt asteroids show a gradation in spectral properties with distance from the Sun (Gradie and Tedesco 1982) suggesting differences in composition or degree of thermal processing. Asteroids in the inner belt tend to be S types which are thought to be dry and rich in iron-magnesium silicates, or M types, some of which may be the parent bodies of iron meteorites. The middle belt is dominated by C types and related classes, many of which have spectral features suggesting they contain hydrated silicates (Rivkin et al. 2003) which probably formed by reactions between water ice and dry rock. The outer belt and Trojan asteroids are P and D types showing no signs of hydrated silicates, although they may contain water ice. Several asteroids in the outer belt display comet-like activity, suggesting they contain some ice (Hsieh and Jewitt 2006).

Meteorites have undergone various degrees of thermal processing and aqueous alteration due to reactions with water. Some carbonaceous chondrites contain up to 10% water by mass in the form of hydrated silicates. Ordinary chondrites contain little water and are more depleted in moderately volatile elements, but there are hints that water was once present (Grossman et al. 2000). Ordinary chondrites have also undergone thermal metamorphism. Primitive achondrite meteorites come from parent bodies that have partially melted, but many were clearly once similar to chondrites. Finally, most iron meteorites and some achondrites come from asteroids that have completely melted and differentiated. The wide range of thermal histories seen in meteorites probably reflects differences in the time of formation and the corresponding degree of heating due to short-lived radioactive isotopes, as well as differences in the initial amount of water ice they contained.

The oxidation state of the solar nebula probably changed over time and with location. At early times, boulder-sized bodies would have drifted inwards across the ice line, evaporating, and increasing the O/H ratio of the gas (Ciesla and Cuzzi 2006). In a turbulent disk, water vapor from the inner disk would have diffused outwards across the ice line potentially depositing large amounts of water ice at a "cold trap" (Stevenson and Lunine 1988). Eventually, much of water became locked up in large planetesimals and embryos, shutting off the flow of boulders and making the inner disk chemically reducing. This may explain differences in chondrite chemistry: the CM and CI carbonaceous chondrites are relatively oxidized, ordinary chondrites are more reduced, while enstatite chondrites are highly reduced, containing nitrides and silicon-bearing metal (Weisberg et al 2006). The removal of water vapor from the inner nebula may also mean that late-forming planetesimals in the asteroid belt contained little water ice, even though they were beyond the ice line at this point (Figure 4).

Terrestrial planets are more depleted in moderately volatile elements than chondrites, while some achondrites are more highly depleted still (Halliday and Porcelli 2001). This suggests that volatile materials escaped as planetary embryos were heated during impacts and by radioactive decay of short-lived isotopes. The isotopic ratios of some noble gases in Earth's atmosphere are enriched in heavier isotopes, arguing that much of the original complement of these elements escaped into space, preferentially leaving heavy isotopes behind (Pepin 2006). Earth may have lost other volatile materials at the same time. The Moon is highly depleted in volatiles which argues in favour of an impact origin.

Planetary embryos the size of Mars or larger are likely to melt and differentiate as a result of the kinetic energy released during impacts with other large bodies (Tonks and Melosh 1992). Iron and other siderophile elements sink to the centre of these bodies, leaving a silicate-mantle surrounding a metal-rich core. Highly siderophile elements like iridium should have been almost entirely extracted into the core as Earth differentiated. However, the highly siderophile elements are still present in small amounts in the mantle, and in roughly chondritic ratios (Drake and RIghter 2002). This suggests Earth accreted the last 1% of its mass from a primitive source after core formation was complete, referred to as the "late veneer".

The principal source of Earth's water is uncertain. Earth's water has a D/H ratio 6 times that of the Sun (Robert 2001), suggesting that this hydrogen was not captured directly from the nebula. The ice line in the solar nebula may have been within 1 AU of the Sun near the end of nebula's lifetime, allowing planetesimals to incorporate water ice. However, it seems likely that planetesimals had already finished forming by this point. If water ice was not present in planetesimals at 1 AU it must have come from further out in the disk. Impacts with planetesimals and planetary embryos originating in the asteroid belt and outer solar system are possibilities. The former source is plausible due to the high collision probability of asteroids with Earth, and the fact that the D/H ratio of water in carbonaceous chondrites

TABLE 2
SELECTED NEBULA CONDENSATION TEMPERATURES AT 10^{-4} BAR (FOLLOWING LODDERS 2003, LEWIS AND PRINN 1980)

Mineral	Temperature (K)
Re	1821
ZrO_2	1764
Al_2O_3	1677
$CaTiO_3$	1593
$MgAl_2O_4$	1397
Fe	1357
Mg_2SiO_4	1354
$MgSiO_3$	1316
FeS	704
H_2O	182
$NH_3.H_2O$	131
$CH_4.7H_2O$	78
CH_4	41
CO	25
N_2	22

matches the ratio in Earth's oceans (Morbidelli et al. 2000, Robert 2001).

3. RESEARCH HIGHLIGHTS

3.1 Turbulence Driven Planetesimal Formation

The formation of planetesimals—objects 1–1000 km in size that are large enough to have appreciable gravitational fields—is one of the main unresolved problems associated with planet formation. Traditionally there have been two schools of thought: planetesimals either formed gradually be pairwise collisions between dust grains, or planetesimals formed rapidly by gravitationally instability in a thin dust layer at the midplane of the disk.

Each of these models has encountered severe difficulties in the face of turbulence. In the particle-sticking model, growth is especially difficult for boulder sized bodies, a problem referred to as the "meter-size barrier". For plausible disk turbulence levels, meter-sized particles collide with one another at speeds of tens of m/s. These collisions probably lead to erosion rather than growth. Differential radial drift rates also mean that m-sized bodies collide with smaller objects at speeds of up to 100 m/s. Experiments show that small aggregates of μm-sized dust particles can embed themselves in larger dust aggregates at speeds of at least 25 m/s (Wurm et al. 2005). However, many asteroids are primarily composed of dense mm-sized chondrules. Chondrule aggregates are unlikely to merge at such high speeds, even when coated with dust rims (Ormel et al. 2008).

Turbulence poses an even more severe challenge to the conventional model for gravitational instability. Turbulence levels equivalent to $\alpha \sim 10^{-7}$ and 10^{-4} are sufficient to prevent mm and m-sized particles respectively from settling to a layer thin enough to become gravitationally unstable (Cuzzi and Weidenschilling 2006). Even in an intrinsically laminar nebula, shear instabilities associated with dust settling will generate local turbulence, and this is sufficient to prevent gravitationally instability unless the solid-to-gas ratio is enhanced by two orders of magnitude compared to that in the solar nebula (Garaud and Lin 2004).

In light of these problems, the hunt is on to find a new mechanism for planetesimal formation that can operate in a turbulent environment. Here we will examine two models that have recently been developed that consider the dynamics of mm- and m-sized particles, respectively.

In a turbulent disk, small particles tend to become concentrated in stagnant regions between eddies (Cuzzi et al. 2001). Concentration is most efficient for the smallest eddies whose size is determined by the point at which turbulence is damped by molecular viscosity. These eddies primarily affect mm-sized particles, which have stopping times comparable to the eddy turnover time.

Turbulent concentration is a stochastic process. Eddies continually form and break up, and particles enter and leave dense clumps repeatedly. However, a particle tends to spend more time in regions of high particle density than in the rarified regions in between. High density clumps form less often than low density clumps. In regions of very high particle density, the particles tend to damp down turbulent motions, preventing further concentration. Calculations show that the local solid-to-gas density ratio is ~ 100 in the densest clumps, which is roughly 4 orders of magnitude higher than the average for material in the solar nebula (Cuzzi et al. 2008).

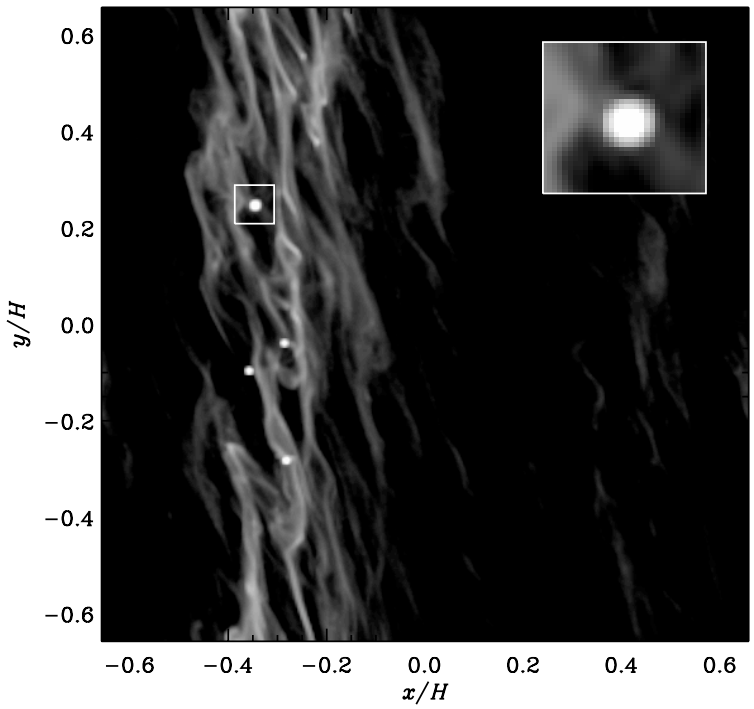

Fig. 5.— A simulation showing the streaming instability involving meter-sized particles in a turbulent disk. The x and y axes refer to the radial and azimuthal directions in the disk, respectively. Brighter shades of grey indicate locations with high particle surface density. The region highlighted by the square box shows a location where a gravitationally bound clump has formed. Figure kindly supplied by Anders Johansen.

Large clumps of particles can be gravitationally bound but they will still have a very low density compared to a planetesimal. Particles are accelerated towards the centre of the clump by gravity. However, particles are also tightly coupled to the gas, so the gas becomes compressed as the particles move inwards, opposing further contraction. Calculations suggest it may take hundreds of orbital periods for mm-sized particles to sediment to the centre of a clump at roughly terminal velocity (Cuzzi et al. 2008).

Particles in dense clumps drag along the gas so that the clump as a whole orbits the star at roughly the Keplerian velocity. Gas in the surrounding region typically moves at sub-Keplerian speeds due to the outward radial pressure gradient in the disk. As a result, a clump is potentially vulnerable to disruption by ram pressure associated with this difference in velocity. Ram pressure increases with the surface area of the clump, while the gravitational binding energy increases with its mass. This implies there is likely to be a minimum mass for a clump that can survive, equivalent to a solid planetesimal with radius of 10–100 km (Cuzzi et al. 2008).

The turbulent concentration model is still at a relatively early stage of development, but it has several appealing features in light of the observed characteristics of primitive meteorites. Surviving clumps should eventually shrink to form planetesimals composed of loosely compacted mm-sized particles similar to chondrite parent bodies. These particles are size sorted during the turbulent concentration phase and are likely to have a narrow size distribution, another property shared by chondritic meteorites (Cuzzi et al. 2001). Finally, the stochastic nature of turbulence, and the fact that high density clumps have a relatively low probability of formation, means that turbulent concentration can naturally explain why planetesimal formation continued in the asteroid belt for several My.

If a large fraction of the dust in a disk becomes incorporated into meter-sized boulders, a second possible route to planetesimal formation arises. Meter-sized objects are strongly affected by gas drag so they quickly move radially towards temporary pressure maxima in a turbulently evolving disk (Johansen et al. 2006). The short radial drift timescale means that these objects can undergo significant concentration before the pressure maximum disappears.

Once the density of boulders is enhanced in a particular region, the particles begin to affect the motion of the surrounding gas. In general, gas orbits the star more slowly than a large solid body due to its outward pressure gradient. As the solid particles become concentrated they begin to drag the gas along at higher speeds. As a result, the relative velocity between the particles and the gas is reduced, and radial drift rates decline. Boulders further out in the disk continue to drift inwards rapidly as before, so solids tend to accumulate in regions where the solid/gas density ratio is already high. This positive feedback effect, referred

to as the "streaming instability", further enhances the solid-to-gas ratio until gravitationally bound clumps form (Figure 5). Numerical simulations show that such clumps are likely to grow in mass and contract over a few orbital periods due to collisions between particles and gas drag (Johansen et al. 2007).

The streaming instability model is attractive in that it provides a way to form bodies comparable in size to the largest asteroids in a vigourously turbulent disk. A necessary prerequisite is that a substantial fraction of the solid material in the disk forms into meter-sized objects. Whether or not this happens, and whether these objects survive mutual collisions in the turbulent disk depends on their mechanical properties, which are poorly constrained at present. An obvious shortcoming of the model is that primitive meteorites are typically composed of mm-sized particles rather than larger objects, although it is conceivable that chondrules first aggregated into roughly meter-sized boulders and these objects subsequently formed planetesimals.

3.2 Radioisotope Dating of Planetary Growth

Theories for planet formation can be tested or constrained using data from radioactive isotope systems to measure timescales. Useful isotope systems fall into two categories. Long-lived isotopes such as ^{238}U were present when rocks formed early in the Solar System, and their decay products can be used to measure the absolute time that has elapsed since these rocks formed. Short-lived isotopes such as ^{26}Al have half lives comparable to timescales involved in planet formation, and they were present in the solar nebula. These isotopes have all decayed now, but the distribution of their daughter isotopes can tell us about the relative timing of different events during planet formation.

For a long-lived isotope system such as Rb-Sr, the number of atoms of the daughter isotope ^{87}Sr increases over time t as the number of atoms of the parent ^{87}Rb declines:

$$\frac{^{87}\mathrm{Sr}(t)}{^{86}\mathrm{Sr}} = \frac{^{87}\mathrm{Sr}(0)}{^{86}\mathrm{Sr}} + \frac{^{87}\mathrm{Rb}(t)}{^{86}\mathrm{Sr}}[\exp(\lambda t) - 1] \qquad (51)$$

where λ is the decay constant which is related to the half life. Here, ^{86}Sr is the number of atoms of another stable isotope of the daughter element not involved in radioactive decay, which is used for comparison.

This equation contains 2 unknowns: the time that has elapsed since the sample formed, and the original amount of the daughter isotope. However, by plotting the current isotopic ratios for different minerals in the same sample, having different elemental ratios, it is possible to determine both quantities. An implicit assumption is that the rocks have remained closed systems. If the system has been disturbed by mixing with other reservoirs, the accuracy of the age estimate will be compromised.

Among long-lived isotopes, the U-Pb system is most widely used. Uranium has two long-lived isotopes ^{235}U and ^{238}U that each decay into a different isotope of lead. The corresponding half lives are 0.7 and 4.5 Gy, respectively, which are convenient for dating events comparable to the age of the Solar System. In addition, the presence of two isotopic clocks running concurrently means it is possible to obtain useful dates even in systems that have been disturbed. A variant of this technique is the Pb-Pb method in which the age of a sample is deduced from measurements of lead isotopes alone, making use of the fact that the two uranium isotopes decay into lead at different rates.

The U-Pb system was the first to be used to measure the age of bodies in the Solar System. More recent measurements have obtained very precise ages for calcium-aluminium-rich inclusions (CAIs), the oldest known objects that formed in the Solar System: 4567.2 ± 0.1 My (Amelin 2006). Lead-lead measurements of rocks on Earth show that it must have formed roughly 100 My later (Allègre et al. 1995).

A number of short-lived isotopes were present early in the Solar System (see Table 3). The source of these isotopes has been the subject of much debate. Light isotopes such as ^{10}Be may have been synthesized in the solar nebula as dust grains close to the Sun were bombarded with energetic particles. Most isotopes, especially heavy, neutron-rich isotopes, were probably generated in nearby massive stars before being ejected into the interstellar medium, ultimately ending up in the solar nebula.

To make use of these systems, it is necessary to assume that the isotopes were uniformly distributed in the solar nebula so that the isotopic ratios for each element depend only on time. The Mg isotope ratios in bulk chondrites, Earth, the Moon and Mars suggest that ^{26}Al, at least, was uniformly distributed (Thrane et al. 2006). In addition, it appears that ^{60}Fe was uniformly distributed and injected at an early stage (Dauphas et al. 2008). The situation is less clear for some other isotopes, and ^{53}Mn may have been unevenly distributed (Lugmair and Shukolyukov 2001).

The ^{26}Al-^{26}Mg system is particularly useful for chronology since the parent isotope has a half life of only 0.7 My, which makes high precision dating possible, and both parent and daughter isotopes are refractory, reducing the probability that the system will be disturbed. From conservation of $^{26}\mathrm{Al} + ^{26}\mathrm{Mg}$, the isotopic ratios that are observed today are related to those at the time a rock formed by

$$\begin{aligned}\left(\frac{^{26}\mathrm{Mg}}{^{24}\mathrm{Mg}}\right)_{\mathrm{today}} &= \left(\frac{^{26}\mathrm{Mg}}{^{24}\mathrm{Mg}}\right)_{\mathrm{original}} \\ &+ \left(\frac{^{26}\mathrm{Al}}{^{27}\mathrm{Al}}\right)_{\mathrm{original}} \times \left(\frac{^{27}\mathrm{Al}}{^{24}\mathrm{Mg}}\right)_{\mathrm{today}} \qquad (52)\end{aligned}$$

A plot of the isotope ratios measured today, for different minerals in the same sample, gives the $^{26}\mathrm{Al}/^{27}\mathrm{Al}$ ratio at the time the rock formed. By comparing this ratio to the $^{26}\mathrm{Al}/^{27}\mathrm{Al}$ ratio in other objects, it is possible to deduce their relative formation times.

On basis of the Al-Mg system, the oldest solid objects known to have formed in the Solar System are CAIs, which are found in most chondritic meteorites (Figure 6). Many

TABLE 3
SHORT-LIVED ISOTOPES IN THE SOLAR NEBULA (ADAPTED FROM WADHWA ET AL 2007)

Isotope	Half Life (My)	Daughter Isotope
^{41}Ca	0.1	^{41}K
^{26}Al	0.72	^{26}Mg
^{60}Fe	1.5	^{60}Ni
^{10}Be	1.5	^{10}B
^{53}Mn	3.7	^{53}Cr
^{107}Pd	6.5	^{107}Ag
^{182}Hf	8.9	^{182}W
^{129}I	15.7	^{129}Xe
^{244}Pu	82	various
^{146}Sm	103	^{142}Nd

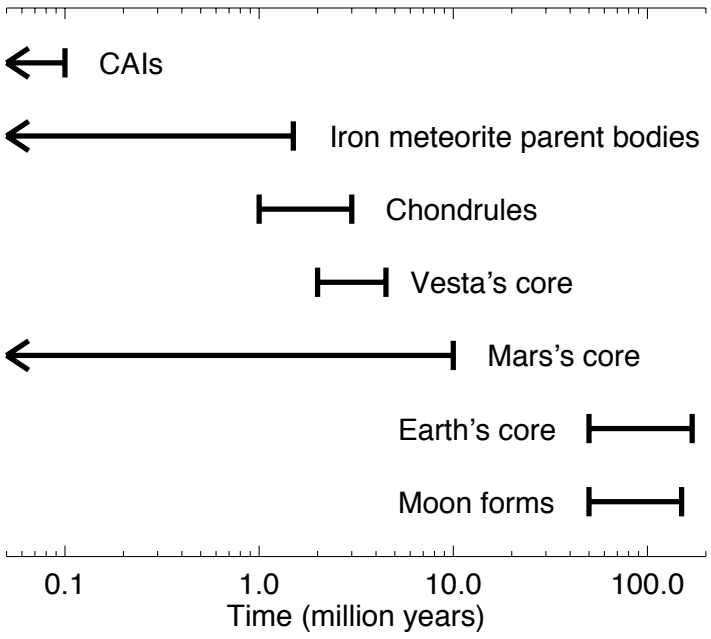

Fig. 6.— Timescales for various events in the early Solar System determined by radioactive isotope dating. Data from Kleine et al. 2002, Halliday 2004, Kleine et al. 2005, Mostefaoui et al. 2002, Nimmo and Kleine 2007, Scott 2007, Touboul et al. 2007, 2008.

CAIs had similar $^{26}\mathrm{Al}/^{27}\mathrm{Al}$ ratios when they formed suggesting they formed over a narrow time interval, possibly as short as 20,000 years (Thrane et al. 2006). The $^{26}\mathrm{Al}/^{27}\mathrm{Al}$ ratio is $\simeq 5 \times 10^{-5}$ for these objects, and this is often assumed to be the ratio shortly after $^{26}\mathrm{Al}$ was synthesized or injected into the solar nebula. Typically, other timescales in cosmochemistry are measured with respect to the time at which these CAIs formed. A few CAIs apparently had little or no $^{26}\mathrm{Al}$ when they formed, which suggests they actually formed even earlier, at a time before $^{26}\mathrm{Al}$ had appeared in the solar nebula (Krot et al. 2008).

Chondrule ages measured using the Al-Mg system are generally 1–2 My younger than CAIs (Mostefaoui et al. 2002), a result that is in excellent agreement with absolute Pb-Pb ages for these objects (Amelin 2006, Connelly et al. 2008). This implies that the chondrite parent bodies formed several My after CAIs. However, the presence of CAIs in most chondritic meteorites implies that some CAIs survived in the nebula for this length of time.

The Al-Mg and Hf-W systems have been applied to the HED meteorites which are thought to come from asteroid 4 Vesta. These analyses show that Vesta must have formed within the first 5 My of the Solar System (Srinivasan et al. 1999, Touboul et al. 2008). Similarly, the angrites, which come from an unidentified differentiated body, formed within 5 My of CAIs (Markowski et al. 2007). The parent bodies of the iron meteorites formed within the first 1.5 My of the Solar System, according to the Hf-W system (Kleine et al. 2005), which means their formation probably predates that of most chondrules.

The Hf-W system is particularly useful for studying differentiated bodies because the parent isotope $^{182}\mathrm{Hf}$ is lithophile, partitioning into the mantle, while the daughter isotope $^{182}\mathrm{W}$ is siderophile, partitioning into the core. The Hf-W system provides a way to date the timing of core formation, and is most easily applied to objects where core formation occurs over a short space of time. For example, the lack of a $^{182}\mathrm{W}$ excess in lunar samples indicates that the giant impact leading to the formation of the Moon happened > 50 My after the start of the Solar System (Touboul et al. 2007).

Caution is required when the Hf-W system is applied to objects like Earth and Mars, where growth and core formation took place concurrently over extended periods of time. A $^{182}\mathrm{W}$ excess has been measured in Earth's mantle (Yin et al. 2002, Kleine et al. 2002). Assuming an exponentially declining rate of growth and complete mixing after each impact event, Earth would have grown to 63% of its final mass in ~ 11 My. This is substantially shorter than calculations based on the Pb-Pb and I-Xe systems (Allègre et al. 1995, Halliday 2004), and estimates based on numerical simulations of planet formation. These numbers can probably be reconciled if it is assumed that only partial mixing occurs during giant impacts (Halliday 2004), although this is still a matter of debate. Similar issues affect age estimates for Mars, in addition to uncertainties about the Hf/W elemental ratio of the planet. However, it appears that Mars formed more rapidly than Earth, within 10 My of CAIs (Nimmo and Kleine 2007).

3.3 N-Body Simulations of Planet Formation

The final stage of terrestrial-planet formation involved a few tens to a few hundred embryos moving on crossing orbits, and lasted $\sim 10^8$ years according to data from radioactive isotopes. The small number of bodies involved and their extensive dynamical interactions means that the kind of statistical analysis often used to study runaway and oligarchic growth is inappropriate here. Instead, this stage is ideally suited to N-body simulations where each object is followed explicitly.

Early studies considered systems of 30–150 embryos, and showed that these typically evolved via dynamical interactions and collisions into a system of 2–4 terrestrial planets on a timescale 100–200 My (Chambers and Wetherill 1998, Agnor et al. 1999, Chambers 2001, Figure 7). The evolution in these simulations is highly stochastic. Many outcomes are possible for similar sets of initial conditions, including differences in the number of planets and their orbits and masses. The prolonged evolution, and large number of close encounters per collision, lead to substantial radial mixing, so that planets like Earth are probably a composite of embryos from throughout the inner Solar System. Potential moon-forming impacts are also commonly seen in these simulations (Agnor et al. 1999).

The results of these early simulations differ from the observed terrestrial planets in two significant ways. Firstly, they tend to produce planets on moderately eccentric orbits, with $e \sim 0.1$, compared to the lower time-averaged values $e \sim 0.03$ for Earth and Venus. Secondly, they fail to reproduce the low mass of Mars and the high concentration of mass seen in the region between 0.7 and 1.0 AU, which contains 90% of the planetary mass interior to Jupiter. Newer simulations involving ~ 1000 planetesimals and embryos have produced terrestrial planets with low eccentricities, more like Earth and Venus (O'Brien et al. 2006, Raymond et al. 2006a). Although planetesimals are continually depleted in these simulations, enough survive for long intervals that dynamical friction with the larger embryos reduces the eccentricities of the latter, resulting in final planets with nearly circular orbits.

N-body simulations of the asteroid-belt region have confirmed the hypothesis that perturbations from the giant planets would dynamically deplete the belt on timescales that are short compared to the age of the Solar System. Simulations involving 15–200 lunar-to-Mars sized embryos find that almost all these objects typically enter resonances due to their mutual interactions, and are subsequently removed from the asteroid belt (Chambers and Wetherill 2001). In roughly 2/3 cases, no embryos survive. Complementary simulations that include test particles find that the loss of embryos is likely to be accompanied by the removal of smaller asteroids, with $\sim 99\%$ of test particles being removed from the asteroid belt in these simulations (Petit et

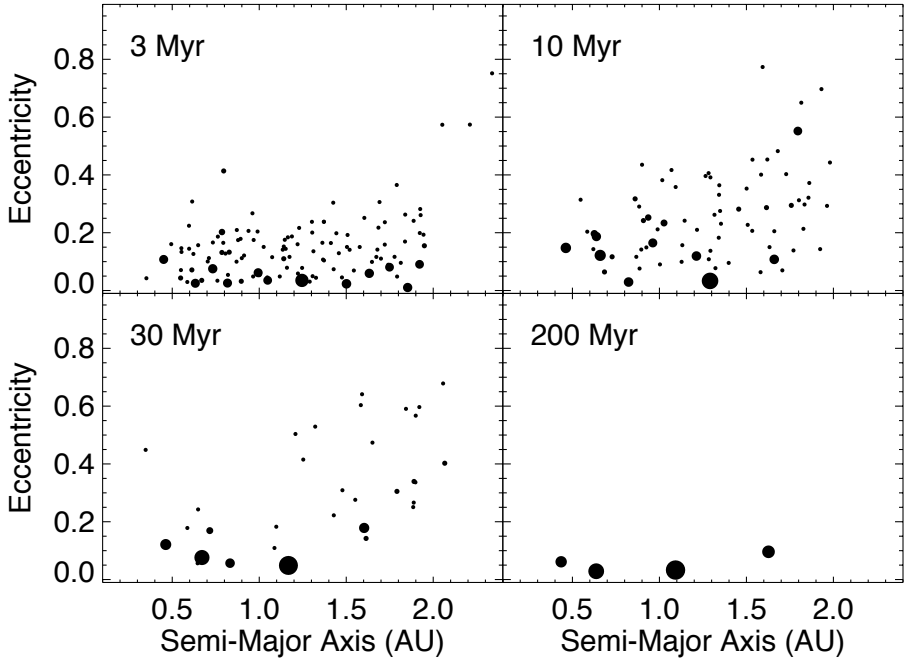

Fig. 7.— A simulation of the final stage of terrestrial planet formation by the author. The simulation begins with 150 lunar-to-Mars mass planetary embryos in the presence of fully formed Jupiter and Saturn. The figure shows 4 snapshots in time. Each circle represents a single planetary embryo with symbol radius proportional to that of the embryo. The largest planet at 200 million years has a mass almost identical to that of Earth.

al. 2001).

Perturbations from giant planets also influence the growth of terrestrial planets outside the asteroid belt. In particular, orbital eccentricities are excited at secular resonances, and this excitation can then be transmitted to neighboring regions by interactions between embryos. The final number of terrestrial planets declines with increasing excitation from the giant planets, with a corresponding increase in the mean planetary mass (Levison and Agnor 2003).

A side effect of the dynamical clearing of the asteroid belt is that planetesimals and embryos develop highly eccentric orbits that cross those of the inner planets. Collisions between these two populations provide one way to deliver water and other volatiles to the terrestrial planets (Morbidelli et al. 2000, Raymond et al. 2006a), although this issue remains controversial. The small number of embryos involved means that the amount of water received by each planet from embryos will vary stochastically from one planet to another. Water delivered by planetesimals should be more uniformly distributed (Raymond et al. 2007). Overall large planets like Earth probably receive more volatiles than smaller planets like Mars (Lunine et al. 2003).

N-body simulations also show that the efficiency of volatile delivery is highly sensitive to the orbital eccentricities of the giant planets, which are poorly constrained at present (Chambers and Wetherill 2001, Chambers and Cassen 2002, O'Brien et al. 2006). When Jupiter and Saturn have eccentric orbits, resonances occupy a large fraction of orbital phase space and these strongly excite the eccentricities of asteroids. As a result, objects in the asteroid belt have short dynamical lifetimes and low collision probabilities with the terrestrial planets. When the giant planets have nearly circular orbits, their perturbations are weaker. The orbits of some embryos in the belt gradually diffuse into the inner Solar System where the chance of hitting one of the inner planets is much higher. Terrestrial planets are likely to be more water rich in this latter case (O'Brien et al 2006).

Simulations that include smooth type-I planetary migration find that this can have a profound effect on planet formation. Many of the embryos initially in the terrestrial-planet region are lost, to be replaced by material from further out in the disk (McNeil et al. 2005, Daisaka et al. 2006). Large embryos migrating inwards can capture smaller objects at an interior mean-motion resonance, so that both objects migrate inwards together at a rate determined by their average mass (McNeil et al. 2005, Cresswell and Nelson 2008). As a result, small objects can be indirectly affected by migration. Migration rates decline over time as the gas dissipates, so late forming embryos and those that migrate inwards from outside the terrestrial-planet region can survive. Migration rates are higher in massive disks, so these may actually be less likely to form terrestrial planets despite having more solid material avail-

able.

In the absence of smooth migration, stochastic tidal torques caused by turbulent density fluctuations tend to excite eccentricities. Tidal damping reduces e while keeping the angular momentum roughly constant, so that $a(1-e^2)$ is unchanged. As a result, a decreases, and embryos move slowly towards the star, even in the absence of conventional type-I migration (Ogihara et al. 2007).

Similarly, embryos probably moved inwards in the Solar System as secular resonances swept across the asteroid belt during the dissipation of the gas disk (Nagasawa et al. 2005). The ν_5 resonance was initially located in the outer main belt when the nebula was present. As it moved inwards, embryos' eccentricities increased, which combined with tidal damping caused the embryos to move inwards. Simulations show that embryos often tend to move inwards at the same rate as the sweeping resonance, transporting large amounts of mass from the asteroid belt to the terrestrial-planet region. As embryos gradually escape from the resonance, their inward motion ceases. Eventually the ν_5 resonance stopped moving when the nebula was completely dispersed, coming to rest in the region now occupied by the terrestrial planets. This "dynamical shake-up" model predicts a pile-up of mass near this final location. It may explain the current concentration of mass between 0.7 an 1.0 AU (Nagasawa et al. 2005, Thommes et al. 2008), but only if the giant planets had their current orbits at this time (O'Brien et al. 2007).

One of the most interesting scenarios examined recently is the possibility that terrestrial planets can form and survive in systems that contain a "hot Jupiter"—that is a giant planet orbiting within ~ 0.1 AU of its star. Hot Jupiters are observed in a number of extrasolar planetary systems. They probably formed in the outer parts of their star's protoplanetary disk and then migrated inwards to their current location due to tidal interactions with the disk. During this migration, planetesimals and planetary embryos in the terrestrial-planet region are either captured into MMRs and shepherded inwards by the giant planet, or they are scattered onto eccentric orbits crossing the outer disk (Raymond et al. 2006b, Fogg and Nelson 2007). Dynamical friction and gas drag subsequently damp the eccentricities of the embryos and planetesimals, respectively. The simulations show that a new disk of material forms beyond the orbit of the migrating giant, and this subsequently evolves into one or more terrestrial planets (Figure 8). These second-generation terrestrial planets typically contain substantial amounts of volatile-rich material from the outer disk, and may be unlike anything in the Solar System.

4. FUTURE PROSPECTS

The next decade should see advances in several areas related to the study of planet formation. Continuing discoveries by the Spitzer infrared space telescope and the upcoming ALMA ground-based mm-wavelength array should greatly improve our knowledge of protoplanetary disks, including their compositions and temporal evolution. The very high spatial resolution of ALMA will provide detailed snapshots of the dust distribution within protoplanetary disks, and should help answer questions about how planets interact with their disks and how disks disperse. The ongoing COROT mission, and recently launched Kepler mission, should provide the first detections of Earth-like planets orbiting other stars like the Sun, and possibly provide compositional constraints. At the same time, further improvements in ground based radial-velocity and transit surveys should continue the inexorable trend towards the discovery of ever lower-mass planets. Searches for planets orbiting low-mass M stars are likely to be particularly fruitful in this respect.

Several relevant space missions are en route to objects in the Solar System. These include the ongoing MESSENGER mission to explore Mercury, which is probably the least understood of the terrestrial planets in the Solar System. The Dawn mission is scheduled to rendez-vous with the two largest main-belt asteroids, Ceres and Vesta, in the coming decade. This will provide an opportunity to compare what we think we know about Vesta on the basis of the HED meteorites with close up observations of their parent body. For Ceres, the prospect is even more enticing since little is known about this dwarf planet including major uncertainties about its formation and composition. At the far end of the Solar System, the New Horizons mission will visit several Kuiper-belt objects including Pluto. While these objects are compositionally very different than Earth, studying them will improve our understanding of the formation of solid planets in general.

Astronomical discoveries are likely to be matched by progress in the field of cosmochemistry. The new generation of secondary ion mass spectrometer (SIMS) probes makes it possible to analyse extremely small samples from meteorites, including matrix grains which have been hard to study previously, as well as samples from comet Wild 2 collected by the Stardust mission. This will improve our understanding of the behaviour of dust grains in protoplanetary disks, and when combined with advances in radiometric dating, should provide strong constraints on the early stages of planet formation. At the same time, ongoing programs to collect meteorites in Antarctica and other remote locations, will expand our sampling of primitive and evolved bodies from the asteroid belt. The likely discovery of new "ungrouped" meteorites will continue to test our theories of what actually happened early in the Solar System.

There is scope for substantial breakthroughs on the theoretical front too. New and rapidly evolving models for the evolution of small particles in turbulent gas suggest we may finally gain a detailed understanding of how planetesimals form, forty years after Safronov first proposed his planetesimal model for planet formation. At the same time, our understanding of what drives the evolution and dispersal of protoplanetary disks is advancing rapidly, and this field is likely to mature substantially over the next ten years. Planetary migration represents a major area of uncertainty at

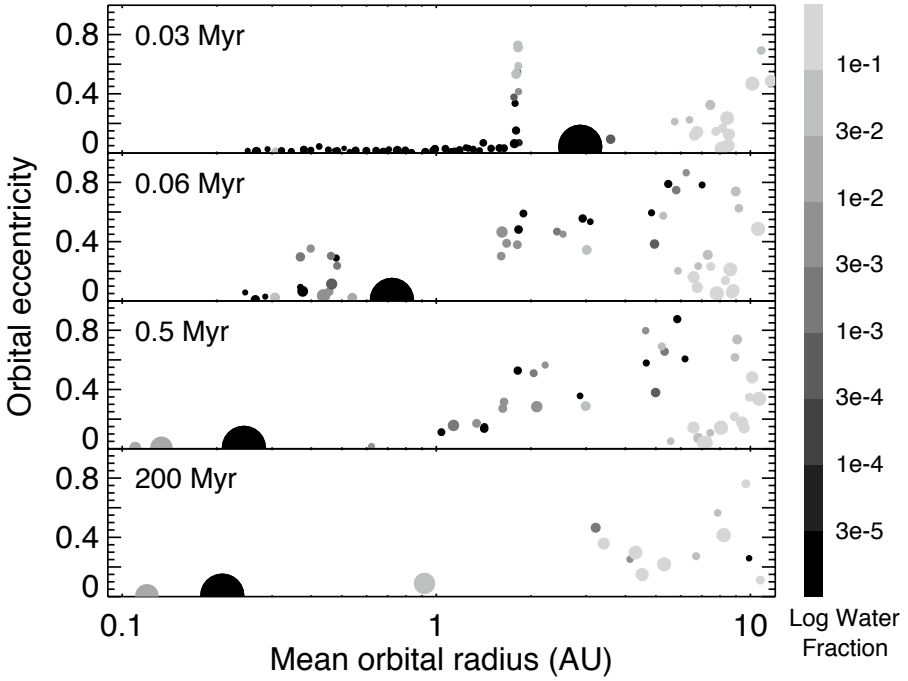

Fig. 8.— Simulation of terrestrial-planet formation in the presence of a migrating gas-giant planet. A Jupiter-mass planet, indicated by the large circle, begins at 5 AU and migrates to 0.25 AU in 10^5 years. The small symbols show planetary embryos, with the embryo's radius proportional to the symbol radius, and the embryo's water mass fraction indicated by the grey scale on the righthand side of the figure. Smaller planetesimals were also included in the simulation but are not shown here. Adapted from Raymond 2006b. Data kindly supplied by Sean Raymond.

present, but a better understanding of the physical processes involved, and continuing improvements in the resolution of hydrodynamical simulations, offer the prospect that we may yet get to grips with this tricky issue. Finally, improved numerical simulations of planet formation, coupled with models for the physical and chemical evolution of planets and protoplanetary disks, should eventually make it clear exactly where Earth's water originated, and what it takes to make a habitable planet.

Acknowledgments. I would like to thank Sean Raymond, Sara Seager, and an anonymous reviewer for helpful comments that helped to improve this article. This work was partially supported by NASA's Origins of Solar Systems program.

REFERENCES

Adachi, I., Hayashi, C. and Nakazawa, K. (1976) The gas drag effect on the elliptic motion of a solid body in the primordial solar nebula. *Prog. Theor. Phys., 56,* 1756-1771.

Agnor, C.B., Canup, R.M. and Levison, H.F. (1999) On the character and consequences of large impacts in the late stage of terrestrial planet formation. *Icarus, 142*, 219-237.

Agnor, C. and Asphaug, E. (2004) Accretion efficiency during planetary collisions. *Astrophys. J., 613*, L157-L160.

Alexander, C.M.O'D, Grossman, J.N., Ebel, D.S. and Ciesla, F.J. (2008) Formation conditions of chondrules and chondrites. *Science, 320*, 1617-1619.

Alexander, R.D., Clarke, C.J. and Pringle, J.E. (2006) Photoevaporation of protoplanetary discs II. Evolutionary models and observable properties. *Mon. Not. Roy. Astron. Soc., 369*, 229-239.

Allègre, C.J., Manhès, G. and Gopel, C. (1995) The age of Earth. *Geochim. Cosmochim. Acta, 59*, 1445-1456.

Amelin, Y. (2006) The prospect of high precision Pb isotopic dating of meteorites. *Meteoritics Plan. Sci., 41*, 7-17.

Asphaug, E. , Ostro, S.J., Hudson, R.S., Scheeres, D.J., and Benz, W. (1998) Disruption of kilometer-sized asteroids by energetic collisions. *Nature, 393*, 437–440.

Benz, W., Slattery, W.L. and Cameron, A.G.W. (1988) Collisional stripping of Mercury's mantle. *Icarus, 74*, 516-528.

Benz, W. and Asphaug, E. (1999) Catastrophic disruptions revisited. *Icarus, 142*, 5-20.

Benz, W. (2000) Low velocity collisions and the growth of planetesimals. *Space Sci. Rev., 92*, 279-294.

Blum, J. and Wurm, G. (2000) Experiments on sticking, restructuring and fragmentation of preplanetary dust aggregates. *Icarus, 143*, 138-146.

Bogard, D.D. (1995) Impact ages of meteorites: a synthesis. *Meteoritics, 30*, 244-268.

Boss, A.P. (1996) Evolution of the solar nebula III. Protoplanetary disks undergoing mass accretion. *Astrophys. J., 469*, 906-920.

Canup, R.M. (2004) Simulations of a late lunar-forming impact. *Icarus, 168*, 433-456.

Canup, R.M. and Asphaug, E. (1999) Origin of the Moon in a giant impact near the end of the Earth's formation. *Nature, 412*, 708-712.

Cassen, P. (1996) Models for the fractionation of moderately volatile elements in the solar nebula. *Meteoritics Plan. Sci., 31*, 793-806.

Chambers, J.E., Wetherill, G.W. and Boss, A.P. (1996) The stability of multi-planet systems. *Icarus, 119*, 261-268.

Chambers, J.E. and Wetherill, G.W. (1998) Making the terrestrial planets: N-body integrations of planetary embryos in three dimensions. *Icarus, 136*, 304-327.

Chambers, J.E. (2001) Making more terrestrial planets. *Icarus, 152*, 205-224.

Chambers, J.E. and Wetherill, G.W. (2001) Planets in the asteroid belt. *Meteoritics, Plan. Sci., 36*, 381-399.

Chambers, J.E. and Cassen, P. (2002) The effects of nebula surface density profile and giant-planet eccentricities on planetary accretion in the inner Solar System. *Meteoritics Plan. Sci., 37*, 1523-1540.

Chambers, J.E. (2006) A semi-analytic model for oligarchic growth. *Icarus, 180*, 496-513.

Ciesla, F.J. and Cuzzi, J.N. (2006) The evolution of the water distribution in a viscous protoplanetary disk. *Icarus, 181*, 178-204.

Connelly, H.C. and Jones, R.H. (2005) Understanding the cooling rates experienced by type II porphyritic chondrules. *Lunar Plan. Sci., 36*, 1881.

Connelly, J.N., Amelin, Y., Krot, A.N. and Bizzarro, M. (2008) Chronology of the Solar System's oldest solids. *Astrophys. J., 675*, L121-L124.

Creswell, P. and Nelson, R.P. (2008) Three-dimensional simulations of multiple protoplanets embedded in a protostellar disc. *Astron. Astrophys., 482*, 677-690.

Cuzzi, J.N., Dobrovolskis, A.R. and Champney, J.M. (1993) Particle-gas dynamics in the midplane of a protoplanetary nebula. *Icarus, 106*, 102-134.

Cuzzi, J.N., Hogan, R.C., Paque, J.M. and Dobrovolskis, A.R. (2001) Size-selective concentration of chondrules and other small particles in protoplanetary nebula turbulence. *Astrophys. J., 546*, 496-508.

Cuzzi, J.N. (2004) Blowing in the wind III. Accretion of dust rims by chondrule-sized particles in a turbulent protoplanetary nebula. *Icarus, 168*, 484–497.

Cuzzi, J.N., Hogan, R.C. and Shariff, K. (2008) Towards planetesimals: dense chondrule clumps in the protoplanetary nebula. *Astrophys. J., 687*, 1432-1447.

Cuzzi, J.N. and Weidenschilling, S.J. (2006) Particle-gas dynamics and primary accretion. In *Meteorites and the Eartly Solar System II* (D.S.Lauretta and H.Y.McSween Jr., eds.), pp353–382, Arizona.

Daisaka, J.K., Tanaka, H. and Ida, S. (2006) Orbital evolution and accretion of protoplanets tidally interacting with a gas disk II. Solid surface density evolution with type-I migration. *Icarus, 185*, 492-507.

Dauphas, N., Cook, D.L., Sacarabany, C., Frohlich, C., Davis, A.M., Wadhwa, M., Pourmand, A., Rauscher, T. and Gallino, R. (2008) Iron 60 evidence for early injection and efficient mixing of stellar debris in the protosolar nebula. *Astrophys. J., 686*, 560-569.

Drake, M.J. and Righter, K. (2002) Determining the composition of the Earth. *Nature, 416*, 39-44.

Durda, D.D., Bottke, W.F., Enke, B.L., Merline, W.J., Asphaug, E., Richardson, D.C., and Leinhardt, Z.M. (2004) The formation of asteroid satellites in large impacts: results from numerical simulations. *Icarus, 170*, 243-257.

Fogg, M.J. and Nelson, R.P. (2007) On the formation of terrestrial planets in hot-Jupiter systems. *Astron. Astrophys., 461*, 1195-1208.

Fromang , S., Terquem, C. and Nelson, R.P. (2005) Numerical simulations of type I planetary migration in non-turbulent magnetized discs. *Mon. Not. Roy. Astron. Soc., 363*, 943-953.

Garaud, P. and Lin, D.N.C. (2004) On the evolution and stability of a protoplanetary disk dust layer. *Astrophys. J., 608*, 1050-1075.

Gladman, B. (1993) Dynamics of systems of two close planets. *Icarus, 106*, 247-263.

Gladman, B.J., Miglorini, F., Morbidelli, A., Zappala, V, Michel, P., Cellino, A., Froeschle, C, Levison, H.F., Bailey, M, and Duncan, M. (1997) Dynamical lifetimes of objects injected into asteroid belt resonances. *Science, 277*, 197-201.

Goldreich, P. and Ward, W.R. (1973) The formation of planetesimals. *Astrophys. J., 183*, 1051-1061.

Gradie, J. and Tedesco, E. (1982) Compositional structure of the asteroid belt. *Science, 216*, 1405-1407.

Greenzweig, Y. and Lissauer, J.J. (1992) Accretion rates of protoplanets. *Icarus, 100*, 440-463.

Grossman, J.N., Alexander, C.M.O'D., Wang, J. and Brearley, A.J. (2000) Bleached chondrules: evidence for widespread aqueous processes on the parent asteroids of ordinary chondrites. *Meteoritics Plan. Sci., 35*, 467-486.

Haisch, K.E., Lada, E.A. and Lada, C.J. (2001) DIsk frequencies and lifetimes in young clusters. *Astrophys. J., 553*, L153-L156.

Halliday, A.N. and Porcelli, D. (2001) In search of lost planets—the paleocosmochemistry of the inner solar system. *Earth Plan. Sci. Lett., 192*, 545-559.

Halliday, A.N. (2004) Mixing, volatile loss and compositional change during impact-driven accretion of the Earth. *Nature, 427*, 505-509.

Hartmann, L. Calvet, N., Gullbring, E. and D'Alessio, P. (1998) Accretion and the evolution of T Tauri disks. *Astrophys. J., 495*, 385-400.

Housen, K.R. and Holsapple, K.A. (1999) Scale effects in strength-dominated collisions of rocky asteroids. *Icarus, 142*, 21-33.

Hsieh, H.H. and Jewitt, J. (2006) A population of comets in the main asteroid belt. *Science, 312*, 561-563.

Hueso, R. and Guillot, T. (2005) Evolution of protoplanetary disks: constraints form DM Tauri and GM Aurigae. *Astron. Astrophys., 442*, 703-725.

Humayun, M. and Clayton, R.N. (1995) Potassium isotope cosmochemistry: genetic implications of volatile element depletion. *Geochim. Cosmochim. Acta., 59*, 2131-2148.

Ida, S. and Makino, J. (1993) Scattering of planetesimals by a protoplanet: slowing down of runaway growth. *Icarus, 106*, 210-227.

Ikoma, M., Nakazawa, K. and Emori, H. (2000) Formation of giant planets: dependences on core accretion rate and grain opacity. *Astrophys. J., 537*, 1013-1025.

Inaba, S. and Ikoma, M. (2003) Enhanced collisional growth of a protoplanet that has an atmosphere. *Astron. Astrophys., 410*, 711-723.

Johansen, A., Klahr, H. and Henning, Th. (2006) Gravoturbulent formation of planetesimals. *Astrophys. J., 636*, 1121–1134.

Johansen, A., Oishi, J.S., Mac Low, M.M., Klahr, H., Henning,

Th., Youdin, A. (2007) Rapid planetesimal formation in turbulent circumstellar disks. *Nature, 448*, 1022-1025.

Kennedy, G.M. and Kenyon, S.J. (2008) Planet formation around stars of various masses: the snow line and the frequency of giant planets. *Astrophys. J., 673*, 502-512.

Kenyon, S.J. and Bromley, B.C. (2006) Terrestrial planet formation I. The transition from oligarchic growth to chaotic growth. *Astron. J., 131*, 1837-1850.

Kleine, T., Münker, C., Mezger, K. and Palme, H. (2002) Rapid accretion and early core formation on asteroids and the terrestrial planets from Hf-W chronometry. *Nature, 418*, 952-955.

Kleine, T., Mezger, K., Palme, H., Scherer, E. and Münker, C. (2005) Early core formation in asteroids and late accretion of chondrite parent bodies: evidence from 182Hf-182W in CAIs, metal-rich chondrites and iron meteorites. *Geochim. Cosmochim. Acta, 69*, 5805-5818.

Kokubo, E. and Ida, S. (1998) Oligarchic growth of protoplanets. *Icarus, 131*, 171-178.

Kokubo, E. and Ida, S. (2000) Formation of protoplanets from planetesimals in the solar nebula. *Icarus, 143*, 15-27.

Krot, A.N., Nagashima, K., Bizzarro, M., Huss, G.R., Davis, A.M., Meyer, B.S. and Ulyanov, A.A. (2008) Multiple generations of refractory inclusions in the metal-rich carbonaceous chondrites Acfer 182/214 and Isheyevo. *Astrophys. J., 672*, 713-721.

Laskar, J. (1997) Large scale chaos and the spacings of the inner planets. *Astron. Astrophys., 317*, L75-L78.

Lecar, M. and Franklin, F. (1997) The solar nebula, secular resonances, gas drag and the asteroid belt. *Icarus, 129*, 134-146.

Levison, H.F. and Agnor, C. (2003) The role of giant planets in terrestrial planet formation. *Astron. J., 125*, 2692-2713.

Lewis, J.S. and Prinn, R.G. (1980) Kinetic inhibition of CO and N_2 reduction in the solar nebula. *Astrophys. J., 238*, 357-364.

Lodders, K. (2003) Solar system abundances and condensation temperatures of the elements. *Astrophys. J., 591*, 1220-1247.

Lugmair, G.W. and Shukolyukov, A. (2001) Early Solar System events and timescales. *Meteoritics Plan. Sci., 36*, 1017-1026.

Lunine, J.I., Chambers, J., Morbidelli, A, and Leshin, L.A. (2003) The origin of water on Mars. *Icarus, 165*, 1-8.

Markowski, A., Quitté, G., Kleine, T., Halliday, A.N., Bizzarro, M. and Irving, A.J. (2007) Hafnium tungsten chronometry of angrites and the earliest evolution of planetary objects. *Earth Plan. Sci. Lett., 262*, 214-229.

Masset, F.S., Morbidelli, A., Crida, A., and Ferreira, J. (2006) Disk surface density transitions as protoplanet traps. *Astrophys. J., 642*, 478-487.

McNeil, D., Duncan, M. and Levison, H.F. (2005) Effects of type-I migration on terrestrial planet formation. *Astron. J., 130*, 2884-2899.

Meibom, A. and Clark, B.E. (1999) Invited review: evidence for the insignificance of ordinary chondrite material in the asteroid belt. *Meteoritics Plan. Sci., 34*, 7-24.

Melosh, H.J. and Ryan, E.V. (1997) Note: asteroids shattered but not dispersed. *Icarus, 129*, 562-564.

Menou, K. and Goodman, J. (2004) Low-mass protoplanet migration in T Tauri alpha disks. *Astrophys. J., 606*, 520-531.

Morbidelli, A., Chambers, J., Lunine, J.I., Petit, J.M., Robert, F., Valsecchi, G.B. and Cyr, K.E. (2000) Source regions and timescales for the delivery of water to the Earth. *Meteoritics Plan. Sci., 35*, 1309-1320.

Mostefaoui, S., Kita, N.T., Togashi, S., Tachibana, S., Nagahara, H. and Morishita, Y. (2002) The relative formation ages of ferromagnesian chondrules inferred from their initial aluminum 26/aluminum 27 ratios. *Meteoritics Plan. Sci., 37*, 421-438.

Murray, C.D. and Dermott, S.F. (2000) Solar System Dynamics. Pub Cambridge University Press.

Nagasawa, M., Tanaka, H. and Ida, S. (2000) Orbital evolution of asteroids during depletion of the solar nebula. *Astron. J., 119*, 1480-1497.

Nagasawa, M., Lin, D.N.C. and Thommes, E. (2005) Dynamical shake-up of planetary systems I. Embryo trapping and induced collisions by the sweeping secular resonance and embryo-disk tidal interaction. *Astrophys. J., 635*, 578-598.

Nelson, R.P. (2005) On the orbital evolution of low mass protoplanets in turbulent, magnetised disks. *Astron. Astrophys., 443*, 1067-1085.

Nesvorný, D., Ferraz-Mello, S., Holman, M., and Morbidelli, A. (2002) Regular and chaotic dynamics in the mean-motion resonances: implications for the structure and evolution of the asteroid belt. In *Asteroids III* (Bottke, W.F., Cellino, A., Paolicchi, P. and Binzel, R.P., eds.), pp379-394, Arizona.

Nimmo, F. and Kleine, T. (2007) How rapidly did Mars accrete? Uncertainties in the Hf-W timing of core formation. *Icarus, 191*, 497-504.

O'Brien, D.P., Morbidelli, A. and Bottke, W.F. (2007) The primordial excitation and clearing of the asteroid belt—revisited. *Icarus, 191*, 434-452.

O'Brien, D.P., Morbidelli, A. and Levison, H.F. (2006) Terrestrial planet formation with strong dynamical friction. *Icarus, 184*, 39-58.

Ogihara, M., Ida, S. and Morbidelli, A. (2007) Accretion of terrestrial planets from oligarchs in a turbulent disk. *Icarus, 188*, 522-534.

Ormel, C.W., Cuzzi, J.N. and Tielens, A.G.G.M. (2008) Co-accretion of chondrules and dust in the solar nebula. *Astrophys. J., 679*, 1588-1610.

Paardekooper, S.J. and Mellema, G. (2006) Halting type I planet migration in non-isothermal disks. *Astron. Astrophys., 459*, L17-L20.

Pahlevan, K. and Stevenson, D.J. (2007) Equilibration in the aftermath of the lunar-forming giant impact. *Earth Plan. Sci. Lett., 262*, 438-449.

Pepin, R.O. (2006) Atmospheres on the terrestrial planets: clues to origin and evolution. *Earth Plan. Sci. Lett., 252*, 1-14.

Petit, J.M., Morbidelli, A. and Chambers, J. (2001) The primordial excitation and clearing of the asteroid belt. *Icarus, 153*, 338-347.

Poppe, T., Blum, J. and Henning, T. (2000) Analogous experiments on the stickiness of micron-sized preplanetary dust. *Astrophys. J., 533*, 454-471.

Raymond, S.N., Quinn, T. and Lunine, J.I. (2007) High-resolution simulations of the final assembly of Earth-like planets. Water delivey and planetary habitability. *Astrobiology, 7*, 66-84.

Raymond, S.N., Quinn, T. and Lunine, J.I. (2006a) High-resolution simulations of the final assembly of Earth-like planets I. Terrestrial accretion and dynamics. *Icarus, 183*, 265-282.

Raymond, S.N., Mandell, A.M., and Sigurdsson. (2006b) Exotic Earths: forming habitable worlds with giant planet migration. *Science, 313*, 1413-1416.

Rivkin, A.S., Davies, J.K., Johnson, J.R., Ellison, S.L., Trilling, D.E., Brown, R.H. and Lebofsky, L.A. (2003) Hydrogen concentrations on C-class asteroids derived from remote sensing. *Meteoritics Plan. Sci., 38*, 1383-1398.

Robert, F. (2001) The origin of water on Earth. *Science, 293*,

1056-1058.

Scott, E.R.D. (2007) Chondrites and the protoplanetary disk. *Ann. Rev. Earth Planet. Sci., 35*, 577-620.

Shakura,N.I. and Sunyaev, R.A. (1973) Black holes in binary systems. Observational appearance. *Astron. Astrophys., 24*, 337-355.

Srinivasan, G., Goswami, J.N. and Bhandari, N. (1999) 26Al eucrite Piplia Kalan: plausible heat source and formation chronology. *Science, 284*, 1348-1350.

Stevenson, D.J. and Lunine, J.I. (1988) Rapid formation of Jupiter by diffusive redistribution of water vapor in the solar nebula. *Icarus, 75*, 146-155.

Tanaka, H., Takeuchi, T. and Ward, W.R. (2002) Three-dimensional interaction between a planet and an isothermal gaseous disk I. Corotation and Lindblad torques and planet migration. *Astrophys. J., 565*, 1257-1274.

Tanaka, H. and Ward, W.R. (2004) Three-dimensional interaction between a planet and an isothermal gaseous disk II. Eccentricity waves and bending waves. *Astrophys. J., 602*, 388-395.

Thommes, E.W., Duncan, M.J. and Levison, H.F. (2003) Oligarchic growth of giant planets. *Icarus, 161*, 431-455.

Thommes, E., Nagasawa, M. and Lin, D.N.C. (2008) Dynamical shake-up of planetary systems II. N-body simulations of solar system terrestrial planet formation induced by secular resonance sweeping *Astrophys. J., 676*, 728-739.

Thrane, K., Bizzarro, M. and Baker, J.A. (2006) Extremely brief formation interval for refractory inclusions and uniform distribution of 26Al in the early Solar System. *Astrophys. J., 646*, L159-L162.

Tonks, W.B. and Melosh, H.J. (1992) Core formation by giant impacts *Icarus, 100*, 326–346.

Touboul, M., Kleine, T., Bourdon, B., Palme, H. and Wieler, R. (2007) Late formation and prolonged differentiation of the Moon inferred from W isotopes in lunar metals. *Nature, 450*, 1206-1209.

Touboul, M., Kleine,T. and Bourdon, B. (2008) Hf-W systematics of cumulate eucrites and the chronology of the eucrite parent body. *Lunar Plan. Sci. 39*, 2336.

Ueda, T., Murakami, Y., Ishitsu, N., Kawabe, H., Inoue, R., Nakamura, T., Sekiya, M. and Takaoka, N. (2001) Collisional destruction experiment of chondrules and formation of fragments in the solar nebula. *Earth Planets Space, 53*, 927-935.

Wadhwa, M., Amelin, Y., Davis, A.M., Lugmair, G.W., Meyer, B., Gounelle, M. and Desch, S.J. (2007) From dust to planetesimals: implications for the solar protoplanetary disk from short-lived radionuclides. In *Protostars and Planets V* (V.B.Reipurth, D.Jewitt and K.Keil eds.), pp835–848, Arizona.

Weidenschilling S.J. (1977) Aerodynamics of solid bodies in the solar nebula. *Mon. Not. Roy. Astr. Soc., 180*, 57-70.

Weidenschilling, S.J. (1980) Dust to planetesimals: settling and coagulation in the solar nebula. *Icarus, 44*, 172-189.

Weidenschilling, S.J. (1997) The origin of comets in the solar nebula: a unified model. *Icarus, 127*, 290-306.

Weisberg, M.K., McCoy, T.J. and Krot, A.N. (2006) Systematics and evaluation of meteorite classification. In *Meteorites and the Eartly Solar System II* (D.S.Lauretta and H.Y.McSween Jr., eds.), pp353–382, Arizona.

Wetherill, G.W. and Stewart, G.R. (1993) Formation of planetary embryos: effects of fragmentation, low relative velocity, and independent variation of eccentricity and inclination. *Icarus, 106*, 190-209.

Wiechert, U., Halliday, A.N., Lee, D.C., Snyder, G.A., Taylor, L.A., Rumble, D. (2001) Oxygen isotopes and the Moon-forming giant impact. *Science, 294*, 345-348.

Woolum, D.S. and Cassen, P. (1999) Astronomical constraints on nebular temperatures: implications for planetesimal formation. *Meteoritics Planet. Sci., 34*, 897-907.

Wurm, G., Paraskov, G. and Krauss, O. (2005) Growth of planetesimals by impacts at $\sim$ 25 m/s. *Icarus, 178*, 253-263.

Yin, Q., Jacobsen, S.B., Yamashita, K., Blichert-Toft, J., Télouk, P. and Albarède, F. (2002) A short timescale for terrestrial planet formation from Hf-W chronometry of meteorites. *Nature, 418*, 949-952.